INVESTIGATION OF THE BOUNDARY CONDITIONS APPLICABLE TO UNDERWATER, AIR-BACKED, FLEXIBLE-DIAPHRAGM TRANSDUCERS

TOBY GENE WARSON

INVESTIGATION OF THE BOUNDARY CONDITIONS APPLICABLE TO UNDERWATER, AIR-BACKED, FLEXIBLE-DIAPHRAGM TRANSDUCERS

by

Toby Gene Warson
Lieutenant Commander, United States Navy
B.S., United States Naval Academy, 1959

Submitted in partial fulfillment of the
requirements for the degree of

MASTER OF SCIENCE IN PHYSICS

from the

NAVAL POSTGRADUATE SCHOOL
June 1968

ABSTRACT

The operation of the MYLAR electrostatic transducer used as a transmitter is studied theoretically and experimentally. A development is made of the mathematical solutions necessary to map the near field patterns generated by a constant velocity circular piston set on an infinite baffle and also a constant pressure piston in the same circumstances.

Boundary conditions applicable to the MYLAR piston are postulated based on equivalent circuits which allow investigation of the theoretical behaviors of the transducer. The postulated boundary conditions are then experimentally investigated. It is shown that an underwater, air-backed, flexible diaphragm transducer very closely approximates a "constant pressure" source.

TABLE OF CONTENTS

LIST OF TABLES

LIST OF ILLUSTRATIONS

LIST OF SYMBOLS

a	radius of source
$U_o e^{i\omega t}$	diaphragm velocity
r, z, t	cylindrical co-ordinates
Φ	acoustic velocity potential
Φ_o	transducer electro-mechanical transfer function
Ψ	spatially-dependent portion of acoustic velocity potential
p	acoustic pressure
ρ_o	density of medium
ρ	density of source material
ω	angular frequency
c_o	speed of sound in medium
c	speed of sound in source material
k	magnitude of the propagation vector $\vec{k}$
$J_n(\zeta)$	Bessel function of the first kind of order n
k_r	r component of the propagation vector k
μ	z component of the propagation vector k
A	area of the acoustic source
Z_m	open-circuit mechanical impedance
C_o	blocked capacitance of transducer
ℓ	thickness of MYLAR film
V	amplitude of signal voltage across transducer

LIST OF SYMBOLS (cont'd)

$p(r)$	local value of acoustic pressure
Z_r	acoustic radiation impedance
(r)	local value of particle velocity
z_r	specific acoustic impedance

ACKNOWLEDGMENTS

The continuing advice and assistance of Professor Alan B. Coppens of the Naval Postgraduate School is gratefully acknowledged.

This research was supported in part by the Naval Ships Systems Command

1. INTRODUCTION

A MYLAR electrostatic transducer is basically a capacitor consisting of a thin, metallized, non-conducting film placed against a solid metal backplate with a small layer of air between the film and the backplate. Bias voltage is applied between the metallized side of the foil and the backplate. Variations in the bias voltage cause the MYLAR film to move normal to the backplate.

In recent years, MYLAR electrostatic transducers have been used in a variety of research projects because they are inexpensive to build, can be manufactured in a variety of configurations, and have responses which are nearly frequency independent when ka is greater than unity [1] . Some work has been done regarding the electromechanical parameters of these transducers but a determination has yet to be made whether this type of transducer is a constant velocity or a constant pressure source.

A constant velocity source is one in which all points on the active face of the transducer move in phase and with constant velocity amplitude. Similarly, a constant pressure is one in which all points on the active face move in phase with constant pressure amplitude.

Many mathematical solutions for the pressure field generated by a constant velocity piston in an infinite baffle have been published [2, 3, 6 7, 8, 9, 10, 11, 12, 13, 15, 17] . An extensive background search revealed no known solutions which could successfully be used to map the near pressure field for either a constant velocity

or a constant pressure piston.

The purposes of this research project were:

(a) to investigate the characteristics of a MYLAR transducer used as a source, and

(b) to develop a mathematical model which would successfully map the near pressure field generated by either a constant velocity or a constant pressure source.

This report describes the present state of solutions describing the near field pressure distributions for a constant velocity circular piston and for a constant pressure circular piston with both pistons mounted on infinite baffles. This report also describes the experimental techniques used in the investigation of the problem, construction of the apparatus used, and a qualitiative summary of the experimental results obtained.

2. THEORY

Development of Theoretical Solutions

The pressure distribution for a constant velocity circular source mounted on a baffle will be developed using the following assumptions:

(a) circular piston of radius a,

(b) piston mounted on a plane rigid baffle of infinite extent,

(c) piston moves uniformly with velocity U_0 normal to the baffle in the z direction, and

(d) cylindrical co-ordinates used with the z-axis perpendicular to the piston at its center and with r normal to z.

The geometry of the problem is shown in Fig. 2.1. Because the baffle is infinite and rigid, the z-component of particle velocity must vanish everywhere on the baffle except over the face of the piston where it has behavior $U_0 e^{i\omega t}$.

Under this condition, the baffle can be replaced by an image source, positioned immediately behind the real source, which radiates an identical acoustic signal into the region of fluid which replaces the baffle and fills the half space which was behind the rigid baffle. The piston and its image can then be replaced by a uniform array of point sources distributed over the surface $r \leq a$ in the $z = 0$ plane. If all of the point sources are in phase, their pulsations

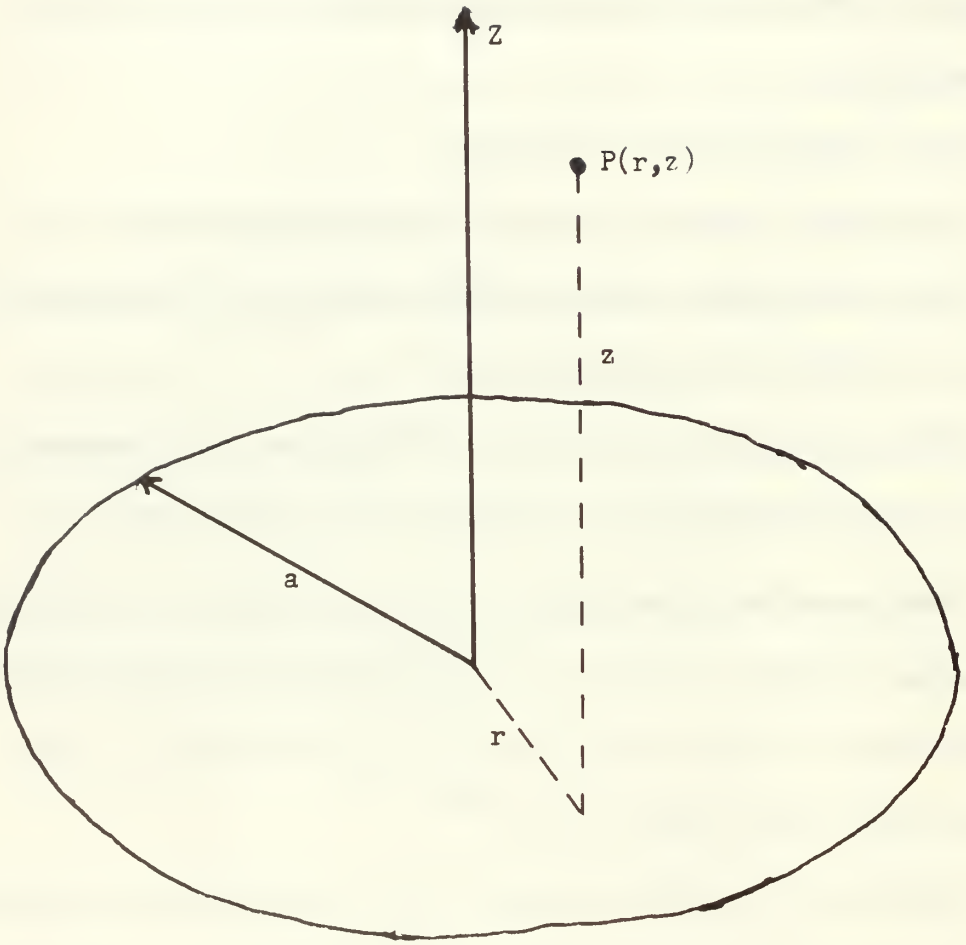

Geometry of a Circular Piston

Cylindrical Co-ordinates

Figure 2.1

will reproduce the velocity behavior of both the piston and its image.

The wave equation

$$\Box^2 \phi = 0$$

where

$$\phi = \psi e^{i\omega t}$$

and where ψ is a function of spatial co-ordinates, becomes the Helmholtz Equation,

$$\nabla^2 \psi = -k^2 \psi \tag{2.1}$$

where

$$k = \frac{\omega}{c} .$$

If discussion is restricted to cylindrical co-ordinates the explicit form of Eq. 2.1 is

$$\frac{\partial^2 \psi}{\partial r^2} + \frac{1}{r}\frac{\partial \psi}{\partial r} + \frac{\partial^2 \psi}{\partial z^2} = -k^2 \psi .$$

Once ϕ (r, z, t) is known, then the acoustic pressure at any point can be found from

$$p = -\rho_0 \frac{\partial \phi}{\partial t}$$

and the particle velocity can be obtained from

$$\vec{u} = \nabla \phi .$$

The appropriate boundary condition for a piston with a rigid diaphragm is

$$u_z(r, z=0) = \left.\frac{\partial \phi}{\partial z}\right|_{z=0} = \begin{cases} U_0 e^{i\omega t} & 0 \le r \le a. \\ 0 & a < r < \infty. \end{cases} \tag{2.2}$$

Lord Rayleigh derived an exact solution for ϕ, [2].

$$\phi = -\frac{1}{2\pi} \iint_A \frac{d\phi}{dz} \frac{e^{-ikp}}{p} \, dA \tag{2.3}$$

In this solution dA is an incremental area on the surface of the piston and p is the distance from the field point P to the surface element dA as seen in Fig. 2.2. Rayleigh's $\frac{d\phi}{dz}$ is identical to $U_0 e^{i\omega t}$ which is the velocity of the diaphragm. This solution is obviously very difficult to handle mathematically. Many scientists and engineers have used Rayleigh's equation as a starting point in an attempt to find approximate or exact solutions.

Louis V. King published an exact integral solution for ϕ in 1934 [3]. This solution, differing in form from Eq. 2.3, is based on the set of eigenfunctions

$$\psi = J_0(k_r r) e^{\pm \mu z} \tag{2.4}$$

which also satisfies Eq. 2.1, where

$$\mu = (k_r^2 - k^2)^{1/2}$$

and k_r is a variable of integration, independent of r and z,

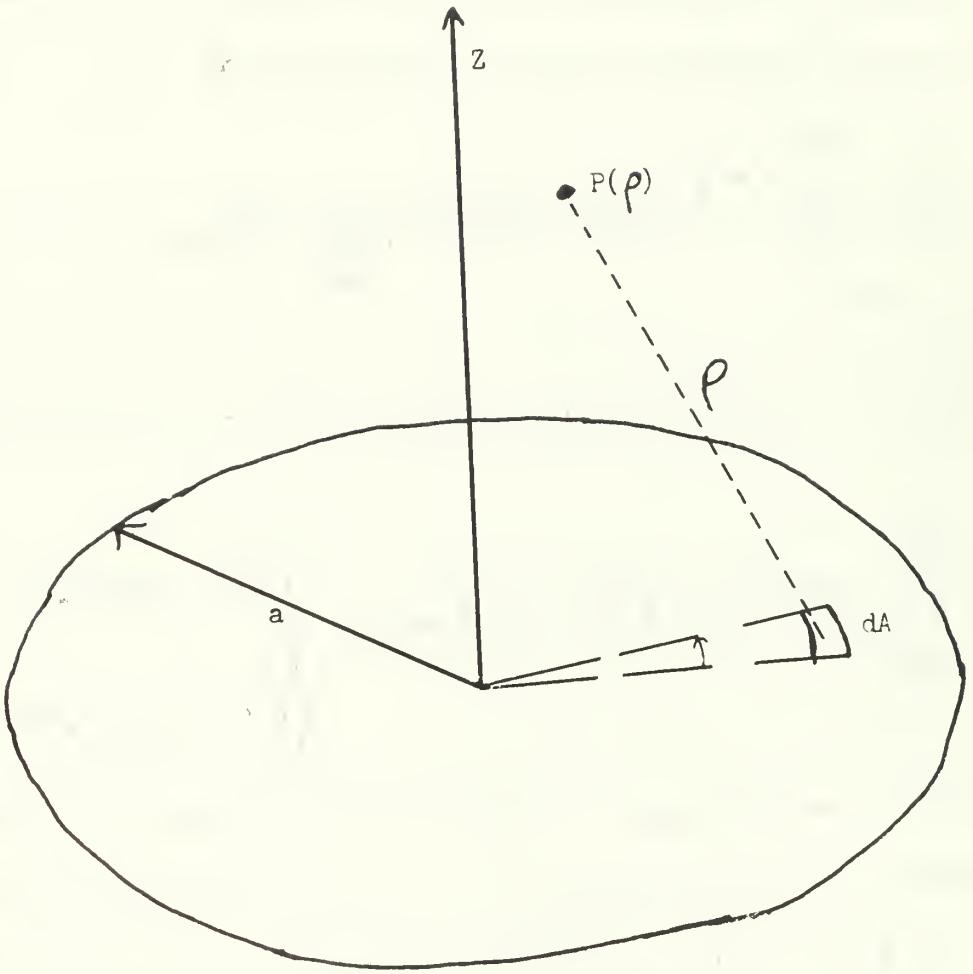

Geometry of a Circular Piston

as Defined by Rayleigh

Figure 2.2

corresponding to the r-component of the propagation vector $\vec{k}$.

King then made use of the fact that any function of k_r multiplied by the solution (Eq. 2.4), is also a solution to the wave equation. Any integration over k_r of such solutions must also be a solution. King thus presented a family of solutions for Ψ as

$$\Psi = \int_0^\infty e^{-\mu z} J_0(k_r r) f(k_r) \frac{k_r}{\mu} dk_r. \tag{2.5}$$

Upon application of boundary conditions, Eq. 2.2, the equation

$$\int_0^\infty \frac{k_r}{\mu} J_0(k_r r) f(k_r) dk_r = \begin{cases} U_0 & 0 \leq r \leq a \\ 0 & a < r < \infty \end{cases} \tag{2.6}$$

results, where $f(k_r)$ is to be determined. King arrived at a solution to Eq. 2.6 by invoking Hankel's inversion theorem which results in

$$f(k_r) = U_0 \int_0^a r J_0(k_r r) dr$$

$$= \frac{U_0 a}{k_r} J_1(ka)$$

By substituting into Eq. 2.5, King's exact solution becomes

$$\phi = a e^{i\omega t} U_0 \int_0^\infty e^{-\mu z} J_0(k_r r) J_1(k_r a) \frac{dk_r}{\mu} \tag{2.7}$$

This solution has been verified as an exact solution to the wave equation [4] . King also in the same paper presented a simplification to his exact solution which was believed valid in the far field. Many math errors have been found in his work [5] but these errors were made after Eq. 2.7 was developed in his paper.

In 1941, Von H. Stenzel published an exact solution which was an expansion of King's integral [6] but valid only for the on-axis situation where r = 0. This solution was very cumbersome. In 1958 Stenzel expanded his solution to include off-axis points [7] . The expanded solution was even more involved than the original and does not readily adapt itself to mapping of the pressure field.

Also in 1941, Von Arnold Schoch [8] published a solution, using Rayleigh's equation as a basis, which has been referenced in many current works. Schoch separated Rayleigh's integral, Eq. 2.3, into two factors, one of which has the form of a plane wave while the other depends on the shape of the piston edge and is called the disturbing or edge wave.

Schoch's solution of

$$\Phi = \frac{i U_0 e^{i\omega t}}{k} \left[\frac{1}{2\pi} \int_0^{2\pi} e^{-ikR(\theta)} \, d\theta \, e^{-ikz} \right]$$

is exact as long as the field point is located in the cylindrical region in front of the piston. Here $R(\theta)$ is the distance from the field

point to the piston edge. This solution requires relocation of the origin to the foot of the perpendicular from the field point to the piston face at a distance x from the center of the piston as seen in Fig. 2.3. Then, in Schoch's notation, $R(\Theta)$ can be written as

$$R(\theta)=\left[z^2+a^2+x^2\cos 2\theta-2x\cos\theta(a^2-x^2\sin^2\theta)^{1/2}\right]^{1/2}$$

This solution has definite possibilities of being numerically integrated using a computer so that the acoustic pressure field could then be mapped.

A. O. Williams of Brown University has published a large number of papers concerning the circular piston in an infinite baffle. In 1945, Williams and Labaw published a fairly simple and accurate approximate solution [9] . This approximate solution was in the form of a series expansion and was valid only for field points near the axis and where $z \gg a$. The year 1951 saw two papers published by Williams. The first paper [10] described an approximate solution for the velocity potential averaged with respect to magnitude and phase over a "measurement circle". This "measurement circle" was equal in area to the piston face and centered in the beam. This solution is of little interest here.

The second paper by Williams published in 1951 presented an exact solution valid for points in the field where $z > a$ [11]. This approach was based on Schoch's work. The solution

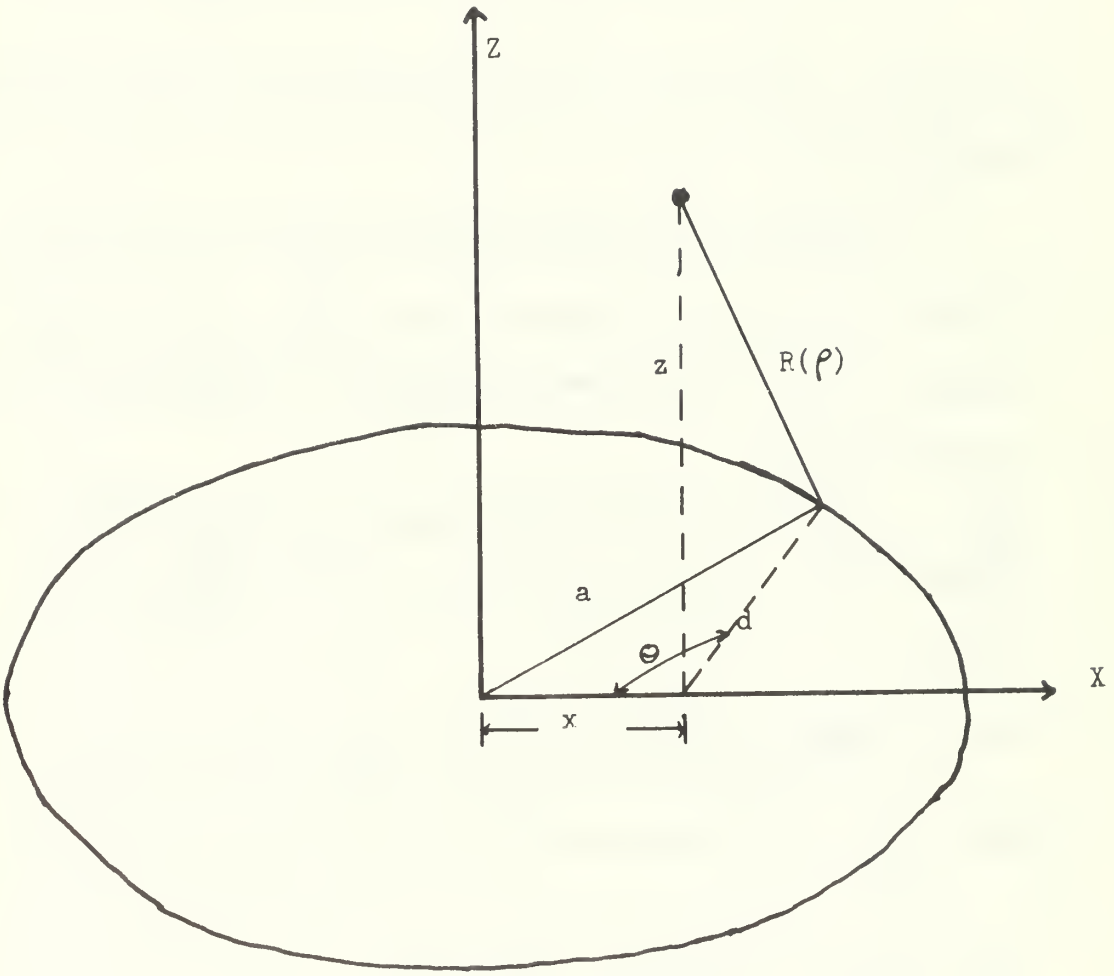

Geometry of a Circular Piston

as Defined by Schoch

Figure 2.3

$$\frac{\Phi}{e^{i\omega t}} = \frac{U_0}{ik} e^{-ikz} - \frac{U_0}{2\pi ik} \sum_{m=0}^{\infty} \frac{(-1)^m}{2^m m!} \left(\frac{k}{2}\right)^m \left(\frac{\pi}{2} kz\right)^{1/2} \tag{2.8a}$$

$$\times H^{(2)}_{m-\frac{1}{2}}(kz) \int_0^{2\pi} \left[r\cos\theta + a\left(1 - \frac{r^2}{a^2}\sin^2\theta\right)^{1/2}\right]^{2m} d\theta$$

is obviously very complicated but is given for the sake of comparison with Eq. 2.8b.

In 1964 Williams published another paper concerning the acoustic field of a circular plane piston [12] . Starting with King's integral, Eq. 2.7, Williams developed a new exact solution for the velocity potential:

$$\frac{\Phi}{e^{i\omega t}} \simeq -\frac{1}{2} i U_0 k a^2 \Lambda_0(krT)\Lambda_1(kaT)\left(\frac{e^{-w}}{w}\right)$$

where

$$w = -ikz, \quad T^2 = (1 - D^2) \quad \text{and} \quad D = \frac{2}{2w} .$$

The Λ'_0 are modifications of the Bessel functions such that

$$\Lambda_n(S) = n! \left(\frac{2}{S}\right)^n J_n(S).$$

Since S is a function of D, it is seen that this equation is an operator form. While of interest mathematically, this equation would seem to be of little practical use.

The latest paper by Williams dealing with the acoustic fields of piston sources was published in 1966. This paper [13] was based

on a portion of King's paper found to be in error by Greenspan [5] . Williams has subsequently published a modification of his earlier paper [14] .

Two other notable solutions have been proposed in the literature. The first of these, published in 1956, was proposed by Seki, Grenato, and Truell from Brown University [15] . Their solution involved use of certain of Lommel's approximation formulas [16] . Starting with Rayleigh's original equation for pressure

$$p = \frac{i\omega\rho_0 U_0}{2\pi} \iint_A \frac{e^{i(kc_0 t - k\rho)}}{\rho} \, dA$$

and splitting it into real and imaginary parts one gets

$$p = \frac{\omega\rho_0 U_0}{2\pi} \iint_A \frac{\sin(kc_0 t - k\rho)}{\rho} \, dA - \frac{i\omega\rho_0 U_0}{2\pi} \iint_A \frac{\cos(kc_0 t - k\rho)}{\rho}$$

with the acoustic pressure at point P being the real part. Taking the real part and applying Lommel's method, Seki, Grenato, and Truell arrived at

$$p = \cos(kc_0 t - kz)\left[V_0 \cos\frac{k(r^2+a^2)}{2z} + V_1 \sin\frac{k(r^2+a^2-1}{2z}\right] + \sin(kc_0 t - kz)\left[V_0 \sin\frac{k(r^2+a^2)}{2z} - V_1 \cos\frac{k(r^2+a^2)}{2z}\right]$$

where

$$V_o = \sum_{n=0}^{\infty} (-1)^n \left(\frac{r}{a}\right)^{-2n} J_{2n}\left(\frac{ka\,r}{\partial}\right)$$

and

$$V_1 = \sum_{n=0}^{\infty} (-1)^n \left(\frac{r}{a}\right)^{-2n-1} J_{2n+1}\left(\frac{ka\,r}{\partial}\right)$$

An attempt was made to use this solution for mapping purposes, but with negative results. Numerical evaluation techniques utilizing a computer (IBM-360) did not produce curves which matched those published in the paper by Seki, Granato, and Truell.

In 1958 Robert H. Quint [17] published another approximate solution based on the power series expansion of Williams and Labaw. Since this solution is very complicated and is, at best, an approximation, its usefulness for mapping the near field pressure pattern is felt to be questionable.

The solution which would seem to hold greatest promise for numerical computer integration starts with King's exact solution, Eq. 2.7. The integral has a weak singularity at $k_r = k$ but can be handled.

Breaking the integral at $k_r = k$ and using the change of variables

(A) $k_r = k \sin\theta \qquad \mu = ik\cos\theta \qquad 0 \le k_r \le k$

(B) $k_r = k\cos\theta \qquad \mu = k\sinh\theta \qquad k_r \to k$

separates Eq. 2.7 into two integrals such that $\phi = \phi_a + \phi_b$

where

$$\frac{\phi_a}{e^{i\omega t}} = -iU_0 a \int_0^{\pi/2} e^{-ikz\cos\theta} J_0(kr\sin\theta) J_1(ka\sin\theta)\, d\theta$$

and

$$\frac{\phi_b}{e^{i\omega t}} = U_0 a \int_0^{\infty} e^{-kz\sinh\theta} J_0(kr\cosh\theta) J_1(ka\cosh\theta)\, d\theta$$

The sign of μ in (B) is chosen to represent an exponential decaying in the + z direction and in (A) to represent a wave traveling in the + z direction.

Now, decomposition of ϕ_a into real and imaginary parts results in

$$\frac{\phi_a}{e^{i\omega t}} = -U_0 a \int_0^{\pi/2} \sin(kz\cos\theta)\, J_0(kr\sin\theta) J_1(ka\sin\theta)\, d\theta$$

$$-U_0 a \int_0^{\pi/2} \cos(kz\cos\theta)\, J_0(kr\sin\theta) J_1(ka\sin\theta)\, d\theta$$

Recombining the real and imaginary parts of both ϕ_a and ϕ_b and letting $\frac{\Phi}{e^{i\omega t}} = R + iI$ leads to

$$R = U_0 a \int_0^{\infty} e^{-kz\sinh\theta} J_0(kr\cosh\theta) J_1(ka\cosh\theta)\, d\theta$$

$$- U_0 a \int_0^{\pi/2} \sin(kz\cos\theta)\, J_0(kr\sin\theta) J_1(ka\sin\theta)\, d\theta$$

$$I = U_0 a \int_0^{\pi/2} \cos(kz\cos\theta)\, J_0(kr\sin\theta) J_1(ka\sin\theta)\, d\theta.$$

The final result for pressure is

$$p = \rho_0 |\dot{\phi}| = a \rho_0 \omega |U_0 e^{i\omega t}| \{R^2 + I^2\}^{1/2} \tag{2.8b}$$

which is seen to be much easier to handle than Eq. 2.8a.

An attempt was made to numerically evaluate the on-axis solution ($r = 0$) using the IBM 360 computer. The IBM library subroutines utilized in this attempt did not provide sufficiently accuracy for successful evaluation. The computer-generated results did not match valid known solutions. Without a good fit for the on-axis situation, little faith could be placed in the computer generated acoustic pressure for the near field region off-axis. The lack of time necessarily precluded further investigation of a computer program to properly numerically evaluate the solution.

Some preliminary work has been done on the pressure field resulting from a constant pressure source [18].

Using boundary conditions such that when $z = 0$, one obtains

$$p = p_0 \qquad 0 \leq r \leq a.$$

$$p = 0 \qquad a < r < \infty.$$

Again, as in King's solution, one family of solutions to the Helmholtz Equation is Eq. 2.5. By making use of the boundary conditions assumed above it is easily seen that

$$\psi = \begin{cases} -\dfrac{p_0}{i\omega\rho_0} & 0 \leq r \leq a. \\ 0 & a < r < \infty. \end{cases}$$

Use is made of the Hankel transform pair

$$f(r) = \int_0^\infty g(k)\, J_0(kr)\, k\, dk$$

$$\Updownarrow$$

$$g(k) = \int_0^\infty f(\rho)\, J_0(k\rho)\, \rho\, d\rho$$

to show that

$$f'(k_r) = \frac{f(k_r)}{\mu} = -\frac{\rho_0}{i\omega\rho_0} \int_0^\infty J_0(k_r r)\, r\, dr = \frac{\rho_0}{i\omega\rho_0} \int_0^a J_0(k_r r)\, r\, dr.$$

Solving the above integral equation yields

$$f'(k_r) = -\frac{\rho_0}{i\omega\rho_0} \frac{a}{k_r} J_1(k_r a).$$

Substituting back into the original equation one gets

$$\phi = -e^{i\omega t} \frac{\rho_0 a}{i\omega\rho_0} \int_0^\infty J_0(k_r r)\, J_1(k_r a)\, e^{-i\mu z}\, dk_r$$

as a solution for the velocity potential at a point P in the field resulting from a constant pressure source.

Theory of Operation

The equivalent electrical circuit of the MYLAR transducer used as a source is shown in Fig. 2.4.

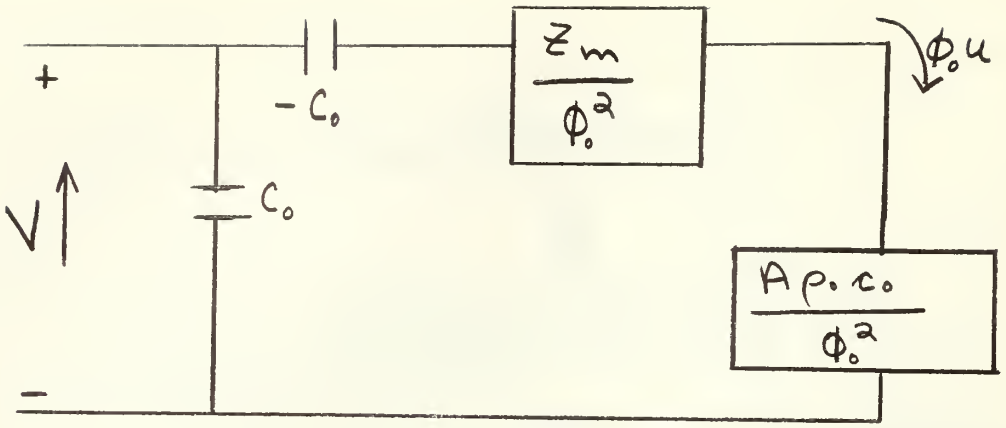

Equivalent Electrical Circuit of a MYLAR Transducer in the Transmitting Mode

Fig. 2.4

Figure 2.5 shows the equivalent circuit of a ceramic transducer, poled in the direction of the applied field, with motion of the ceramic being in the poled direction. The transducer is assumed operating under conditions such that one side of the ceramic is unloaded and the other side is operating into some finite acoustic impedance.

Making the assumption that these transducers operate with uniform velocity over the acoustically active faces, one can then treat each face as a rigid diaphragm. The diaphragm is assumed to be moving harmonically with velocity $u = U_0 e^{i\omega t}$ in Figs. 2.4 and 2.5. Both transducers are assumed to be highly directive (an assumption which is valid for the transducers used in this research paper); therefore, the radiation impedance Z_r across the face of the transducer can be approximated by

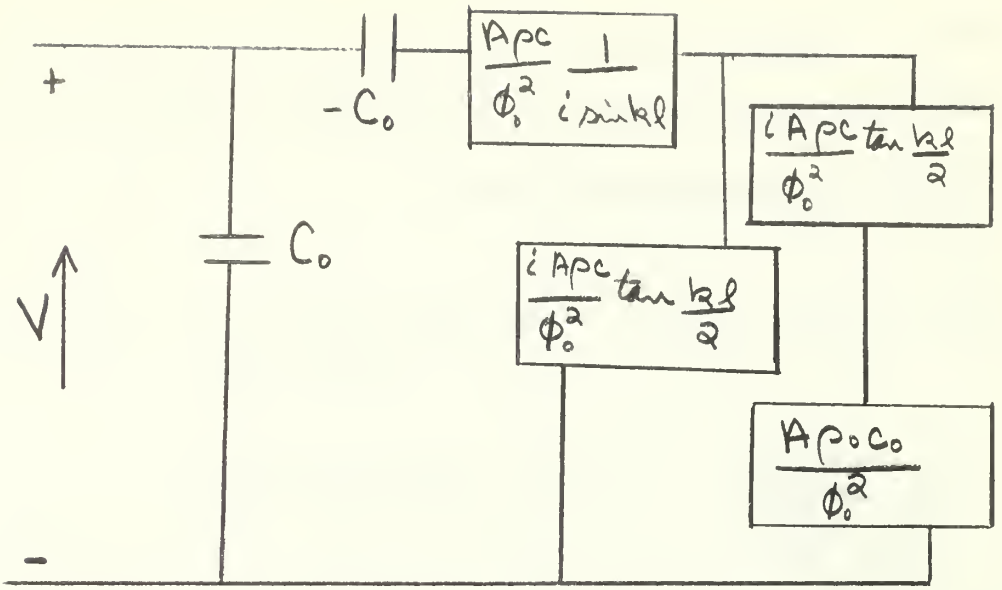

Equivalent Electrical Circuit of a Ceramic Transducer in the Transmitting Mode

Fig. 2.5

$$Z_r \doteq A \rho_0 c_0$$

where

A = area of the active face

ρ_0 = density of the fluid in which the transducer is immersed

c_0 = speed of sound in the fluid

The radiation impedance Z_r is defined as [19].

$$Z_r = \frac{1}{U_0} \int_A P(r)\, dA \qquad (2.9)$$

where

dA = incremental area of the active face and

$$p(r, z = o) = P(r)\, e^{i\omega t}$$

Representative values for the two types of transducers, both of the same dimensions and operating at a frequency for which $ka \stackrel{\Delta}{=} 30$, are given in Table 2.1.

MYLAR Transducer

$\left\lvert \frac{Z_m}{\Phi_0^2} \right\rvert$	=	1.72×10^4 ohms
$\left\lvert \frac{A\rho_0 c_0}{\Phi_0^2} \right\rvert$	=	1.19×10^5 ohms
$\left\lvert \frac{1}{i\omega C_0} \right\rvert$	=	3.92×10^2 ohms

Ceramic Transducer

$\left\lvert \frac{A\rho c}{\Phi_0^2} \frac{1}{i \sin kl} \right\rvert$	=	3.33×10^4 ohms
$\left\lvert \frac{A\rho c}{\Phi_0^2} i \tan \frac{kl}{2} \right\rvert$	=	6.53×10^4 ohms
$\left\lvert \frac{1}{i\omega C_0} \right\rvert$	=	186.8 ohms
$\left\lvert \frac{A\rho_0 c_0}{\Phi_0^2} \right\rvert$	=	9.3 ohms

Representative Values for Equivalent Electrical Circuits

Table 2.1

Examination of Fig. 2.4 and Table 2.1 reveals that the radiation impedance Z_r is the dominant impedance on the mechanical side of the equivalent circuit for the MYLAR transducer. With the radiation impedance completely swamping both the mechanical impedance and also the impedance due to the negative capacitance C_o, the approximation $V \doteq u(r) Z_r$ may been seen to follow.

On the other hand, examination of Fig. 2.5 and Table 2.1 for the ceramic transducer shows that the mechanical impedance is very much the dominant impedance. Thus, one can safely conclude that the velocity u(r) is virtually independent of the radiation impedance for the ceramic transducer. Using Eq. 2.9 and this conclusion, the ceramic transducer appears to be virtually independent of the local value of pressure, p(r).

The two transducers have substantially different characteristics regarding their dependences upon their respective radiation impedances. The action of MYLAR transducer appears to depend strongly on the local value of p(r). In order to investigate the differences between the two transducers more fully, the areas of the active faces of both transducers are imagined to be divided into n equal smaller areas. A small incremental area Δ A is defined as

$$\Delta A = \frac{A}{n}$$

where each small element of area Δ A sees an acoustic loading

equal to the incremental radiation impedance ΔZ_r which is defined as

$$\Delta Z_r = \mathfrak{Z}_r(r)\,\Delta A \tag{2.11}$$

where $\mathfrak{Z}_r$ is the specific acoustic impedance, defined [19] by

$$\mathfrak{Z}_r = \frac{p(r)}{u(r)}. \tag{2.12}$$

The ceramic transducer has been shown to have velocity almost independent of the acoustic loading so that it is clearly a "uniform velocity source". Thus the velocities of the incremental areas are not affected by the local changes in acoustic impedance in the fluid caused by the motion of adjacent incremental areas. This uniform velocity of all the incremental areas when $ka \gg 1$ requires $p(r)$ to be a strongly varying function.

For the MYLAR transducer, however, it has been shown that the velocity of the transducer face is almost entirely dependent upon the radiation impedance present at the face. It can thus be assumed that the velocities of the incremental areas over the face of the MYLAR piston are dependent upon the variations in the local radiation impedance, ΔZ_r as seen by the incremental areas. These variations in values of the radiation impedance are due to the motions of the adjacent incremental areas. Since the potential V across each of the incremental areas is equal and, since for the MYLAR transducer $V \doteq Z_r u(r)$, the velocities for the individual areas

can be expressed as

$$u(r) \doteq \frac{V}{\Delta z_r} \,. \tag{2.13}$$

Substituting Eq. 2.12 into Eq. 2.11 reveals

$$\Delta z_r = \frac{p(r)}{u(r)} \Delta A$$

which, when substituted into Eq. 2.13, reveals

$$p(r) \propto V \tag{2.14}$$

Since V is constant, Eq. 2.14 leads one to reason that the MYLAR transducer closely resembles a constant pressure source.

3. EXPERIMENTAL EQUIPMENT

MYLAR Transducers

MYLAR (registered trademark) is a polyester film manufactured by Dupont and can be purchased in different thicknesses with either an aluminum or gold coating on one surface. All of the MYLAR material used during this research project was one-mil thick and had an aluminum coating on one surface.

The first of the MYLAR transducers constructed utilized lucite as the primary construction material with aluminum used as the backplate as shown in Fig. 3.1. The inner aluminum cylinder was included in the design for electromagnetic shielding purposes and was very effective in eliminating electrical pick-up which had been a problem in previous designs. This transducer was an adequate source, but a weak area of the lucite around the support pipe eventually cracked, allowing water to leak into the transducer. The water provided a conduction path between the two electrodes thus shorting out the transducer.

A second MYLAR transducer was constructed using aluminum as the primary construction material. The details of this construction are shown in Fig. 3.2. The small lucite disk between the aluminum backplate and the aluminum support structure was installed to provide electrical insulation between the two aluminum pieces. The air gap around the periphery of the aluminum backplate was included

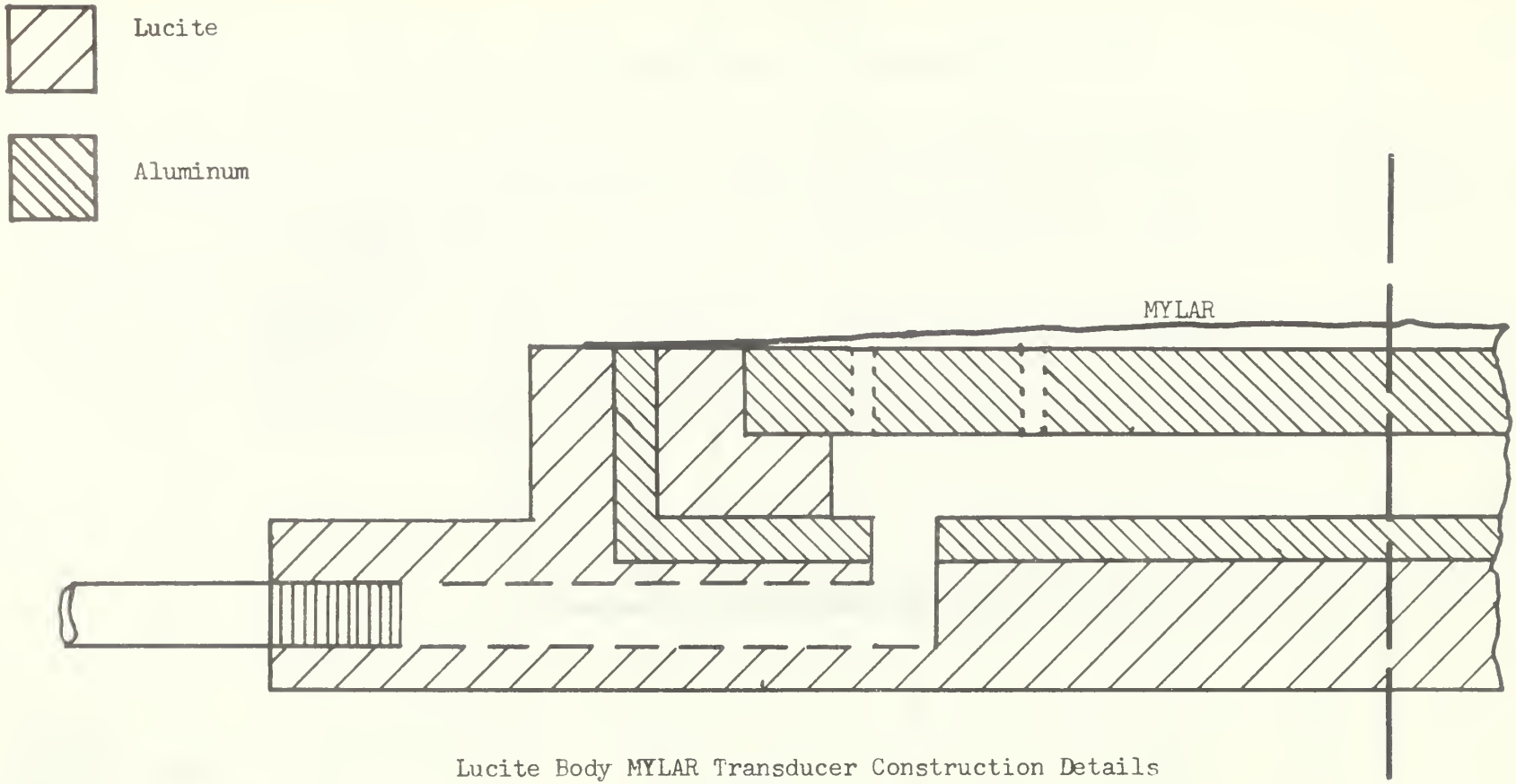

Lucite Body MYLAR Transducer Construction Details

Figure 3.1

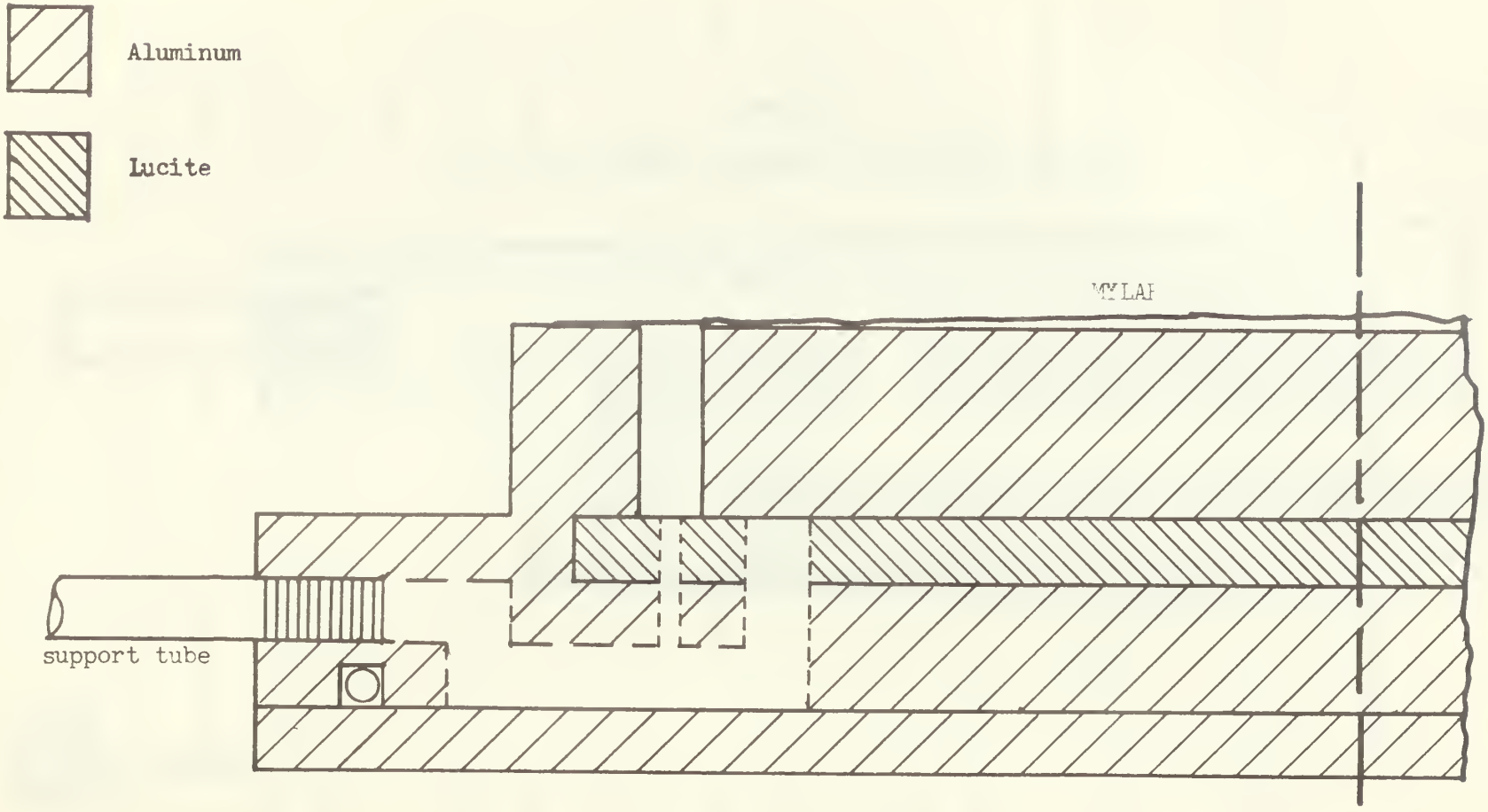

Aluminum Body MYLAR Transducer Construction Details

Figure 3.2

in the design of this transducer to insure positive contact between the MYLAR and the complete surface of the aluminum backplate. An 0-ring was used to provide a water-tight seal between the main structural member and the rear plate. This design proved to be satisfactory in preventing water leakage.

Many different MYLAR faces were installed on the two MYLAR transducers constructed. The replacements were required because of water leakage into one of the transducers and because of gross asymmetries in the pressure patterns produced by both transducers. The asymmetric pressure patterns resulted when the MYLAR was applied with non-uniform tension around the circumference of the circular face. The non-uniform tension resulted from application difficulties. When a transducer was found to have been constructed so that these gross asymmetries occurred, the MYLAR face was replaced.

All of the transducers constructed were designed to be highly directive ($ka \doteq 30$) at the chosen frequency of approximately 100 kHz. This directivity was desired for a variety of reasons: (1) The experiment was conducted in a reverberant tank requiring sound absorbing material to prevent generation of echoes from reflections off the sides of the tank. A high directivity simplified the problem by requiring that the absorbant materials be placed only directly in front of the piston. (2) Since the edge of the transducer was about three wavelengths from the edge of the active face, and the

high directivity guaranteed that there would be extremely small acoustic fields in directions normal to the axis of symmetry of the beam, no other baffle was thought necessary to simulate the theoretical infinite baffle.

Barium Titanate Transducer

The third transducer constructed as a source was one utilizing a ceramic disk as the active element. The ceramic used was Barium Titanate (type HS-21, manufactured by Gulton Industries of Metuchen, New Jersey) [20] in the shape of a disk. The disk was six inches in diameter by one inch thick and consisted of two one-half inch thick disks bonded together by the manufacturer.

Built to the same dimensions as the second MYLAR transducer, this transducer was to have served as a constant velocity source. Nylon-backed foam-neoprene sheet (wet-suit material) was used in place of the plastic insulating insert in the MYLAR transducer to decouple the ceramic from the aluminum housing. The neoprene material was also used to partially fill the gap around the periphery of the ceramic to provide centering support for the ceramic.

The neoprene did not completely fill the space and, thus an air gap was present, similar to the air gap in the MYLAR transducer. Every effort was made to make the Barium Titanate transducer identical to the MYLAR transducer used. All dimensions were the same with the only deliberate difference between the two

transducers being the different acoustically active faces. This was done so that differences in the pressure patterns produced by the two transducers would be attributable only to the material used for the diaphragm.

Tank

The tank used in this experiment was constructed of 1/4 inch sheet steel and measured 10 feet long by 3 feet deep by 4 feet wide. Since the tank was not anechoic, sound attenuating materials were used in the tank to prevent reflections from the sides and bottom of the tank. The directive source was placed mid-length in the tank on the centerline and pointed toward one end of the tank. The end of the tank toward which the source pointed was lined with the attentuating material and the system was checked for reflections as described in the procedure section of this report. The tank was filled to a depth of 30 inches with tap water.

Receivers

Two different receivers were used for this research project, both were of type HS-21 Barium Titanate [20] . For far-field measurements, a 1/4 inch probe was used, and for near-field measurements a 1/8 inch probe was used.

The 1/4 inch probe was a thin-walled cylinder with an outside diameter of 0.250 inches, a length of 0.250 inches, and a wall

thickness of 0.062 inches. The probe was mounted on the end of a 10 foot piece of coaxial cable and supported by a length of 1/8 inch stainless steel rod. It was felt that 1/4 inch probe was appropriate for use in the far field because the point to point fluctuation in the pressure field was not as great as in the near field and the 1/4 inch probe provided greater sensitivity than the 1/8 inch probe in the weaker far field.

The 1/8 inch probe used in the collection of the near field data was a thin-walled cylinder of 0.125 inches in length, wall thickness of 0.030 inches, and outside diameter of 0.125 inches. The probe was mounted on the end of a 10 foot piece of micro-dot cable and again supported by a length of 1/8 inch stainless steel rod. It was deemed appropriate to use a smaller probe for near field pressure measurements because of the rapidly varying point to point pressure patterns encountered in the near field.

Receiver Transport System

In order to automate the data taking and processing, a system was devised to transport the receiving probe across the tank in front of the transducer at a set depth and constant slow speed of 3.0 inches per minute. An aluminum cart 5 inches long by 7/8 inches wide by 1 and 3/8 inches high was mounted on four "slot-car" wheels and held the receiver. The cart traveled on two tracks, spaced about 3 inches apart, which covered the width of the tank.

The cart was driven by the output drive section of a BRUEL and KJAER level recorder through a flexible drive to the driving pulley. As shown in Fig. 3.3, nylon cord was attached to either end of the cart passing over an idler sheave at one end of the tracks, and the driving pulley was on the other end transmitting the motion of the driving pulley to the cart. Rotation of the driving pulley thus caused the cart to traverse the width of the tank. A 10 turn rheostat coupled to the same shaft as the driving pulley provided position information to the X-Y plotter. A Hewlett Packard power amplifier, type 467-A, was used to provide 10 volt D.C. power to the rheostat.

Electronics Equipment

Fig. 3.4 shows the block diagram of the electronics equipment used in this research project. Table 3.1 identifies the components in the figure.

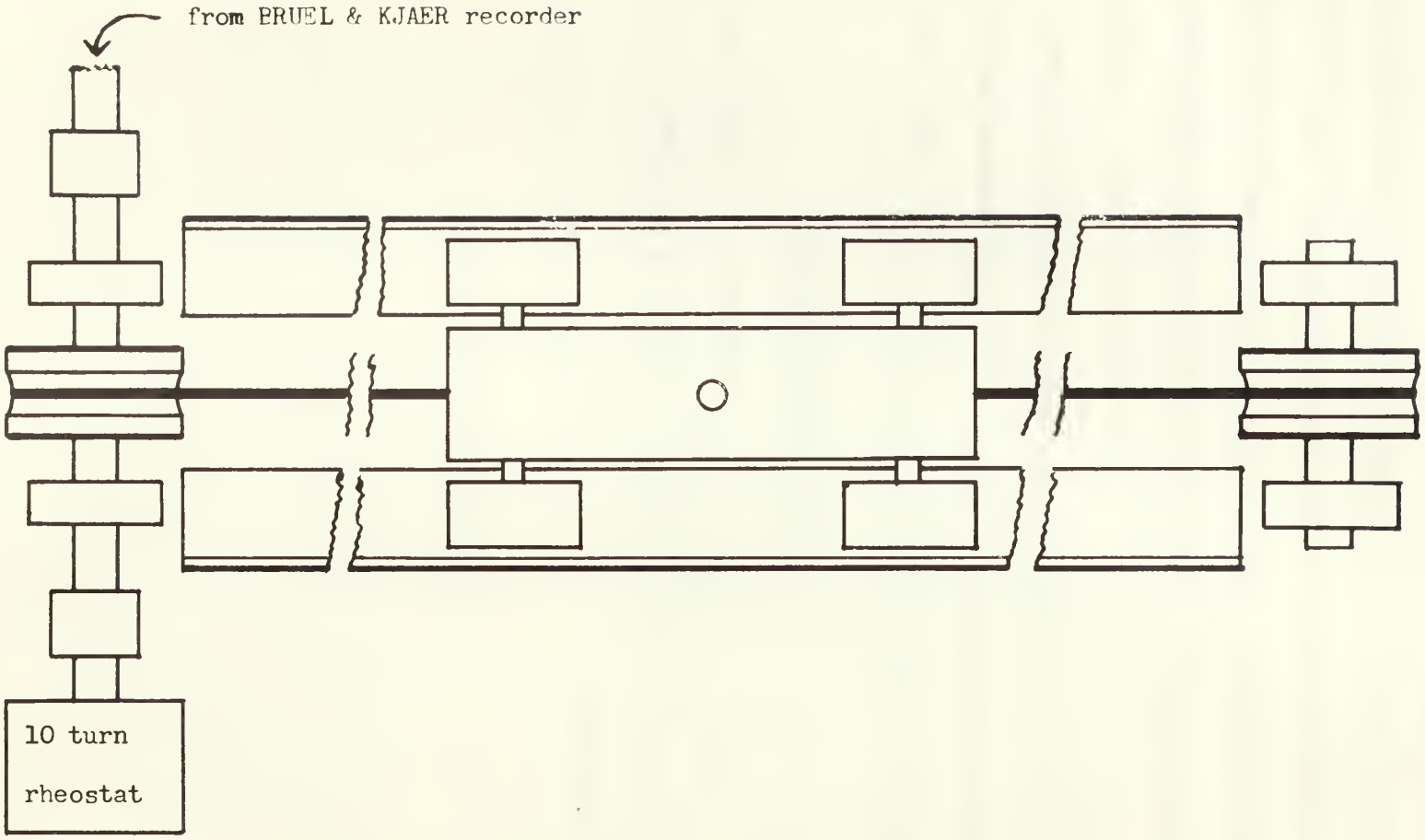

Receiver Transport System

Figure 3.3

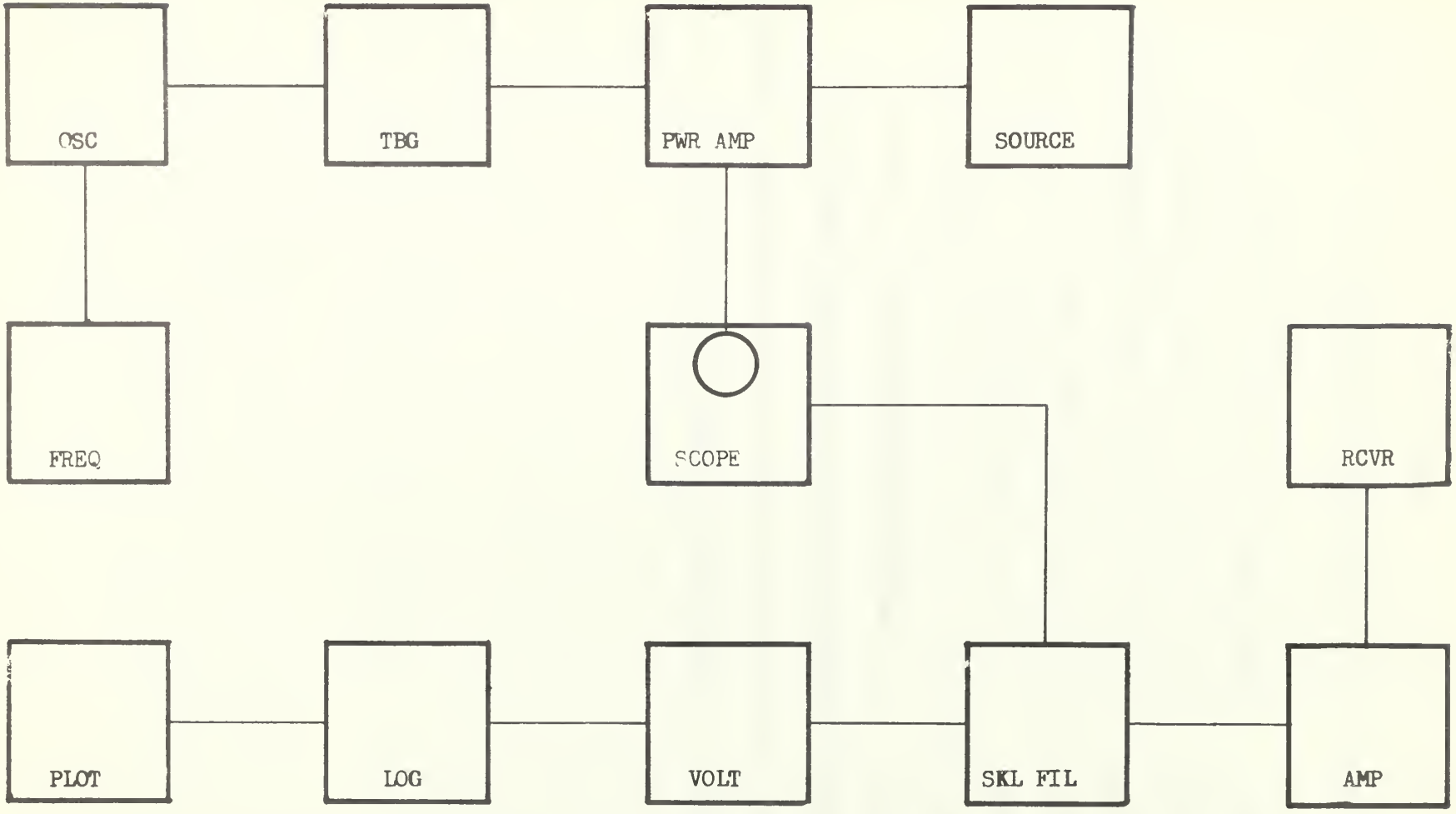

Electronics Equipment

Figure 3.4

Table 3.1

Electronics Equipment

AMP	Voltage amplifier, Tektronix type 1121
FREQ	Electronic counter, Hewlett Packard 5233-L
LOG	Logarithmic converter, Hewlett Packard 7561-A
OSC	Oscillator, General Radio type 1310
PLOT	X-Y plotter, Moseley type 135-C
PWR AMP	Power amplifier, Hewlett Packard 467-A
SCOPE	Dual beam oscilloscope, Fairchild model 777
SKL FIL	Electronic band pass filter SKL model 302
TBG	Tone burst generator, General Radio type 1396-A
VOLT	RMS voltmeter, Hewlett Packard 3400-A

4. EXPERIMENTAL INVESTIGATION

The purposes of the experimental investigation were (a) to obtain plots of the pressure field generated by both the MYLAR and Barium Titanate sources, and (b) using these plots, to determine what type of source the MYLAR transducer was. The pressure field was plotted in both near and far fields. More plots were taken of the near field than the far field because analysis of preliminary plots indicated the existence of greater differences between the two types of sources in the near field region.

Experimental Procedure

With the tank filled to the proper level and the electronics equipment stabilized, the source was placed in a position mid-length in the tank. The source was positioned so that the active face pointed toward one end of the tank. The depth of the source beneath the surface of the water was adjusted so that the major pressure lobe as well as the first and second side lobes would reach the end of the tank before impinging on the water surface. This was done to prevent interference caused by surface reflections. With the source in position, the rod holding the appropriate receiver was positioned in the cart. The tracks holding the cart were then placed across the width of the tank and thus parallel to the active face of the source. The depth of the receiver was then adjusted to the depth of the center of the source.

The source was then operated in a pulsed mode utilizing a gated sine wave produced by the oscillator and tone burst generator. The probe was then moved across the width of the tank and the portable sound absorbing material adjusted so that no reflections from the walls of the tank were present at any position of the receiver. The driving signal and the received signal were both monitored on the dual beam scope during these preliminary adjustments. When all reflections had been reduced to sufficiently small level, the source was then shifted to the CW mode. All plots were taken with a driving frequency of 96.820 $\pm$ .005 kHz, the resonant frequency of the Barium Titanate source. MYLAR sources have been shown to be frequency independent as long as they are operated at frequencies such that $ka \gg 1$ [1]. When operated at a frequency of 96.820 kHz, ka = 31.2; thus, it was judged advisable to operate solely at the resonant frequency of the Barium Titanate transducer.

Prior to actually making the plot, a check was made to ensure that the distance between the plane of the source face and the receiver was unchanging at all points along the path of the receiver. This distance was maintained constant to within $\pm$ 0.1 cm for all plots.

The scale of the X-Y plotter was adjusted so that the probe traveling across the area of interest resulted in a plot of appropriate width. Reference marks were made on all plots to show position of the receiver relative to the source; LHS indicating receiver

directly opposite the left hand side of the active face of the source, C.L. indicating receiver on center line, and RHS indicating receiver directly opposite right hand side. Pressure level reference marks were also included on all plots for analysis purposes. The pressure level reference marks were made by changing the attenuation setting on the logarithmic converter.

After plotting the reference marks and assuming that no reflections were present, the receiver was then positioned at the starting point. The BRUEL and KJAER recorder's flexible drive was attached to the drive shaft, and the plot was made automatically as the cart moved across the tank. The speed of the probe was very slow, approximately 3 inches per minute, so that the system time delays would affect the accuracy of the plots insignificantly.

Analysis of Data Plots

The far field pressure plot of the Barium Titanate source, as shown in Fig. 4.1, clearly demonstrates that the ceramic disk did not produce a symmetric pressure pattern. After investigation, it was found that asymmetric pressure difficulties are not uncommon with ceramic transducers of this size [21].

The far field pressure plot of the MYLAR source, as shown in Fig. 4.2 clearly indicated that the MYLAR source used did not produce a perfectly symmetric pressure field either. The asymmetric

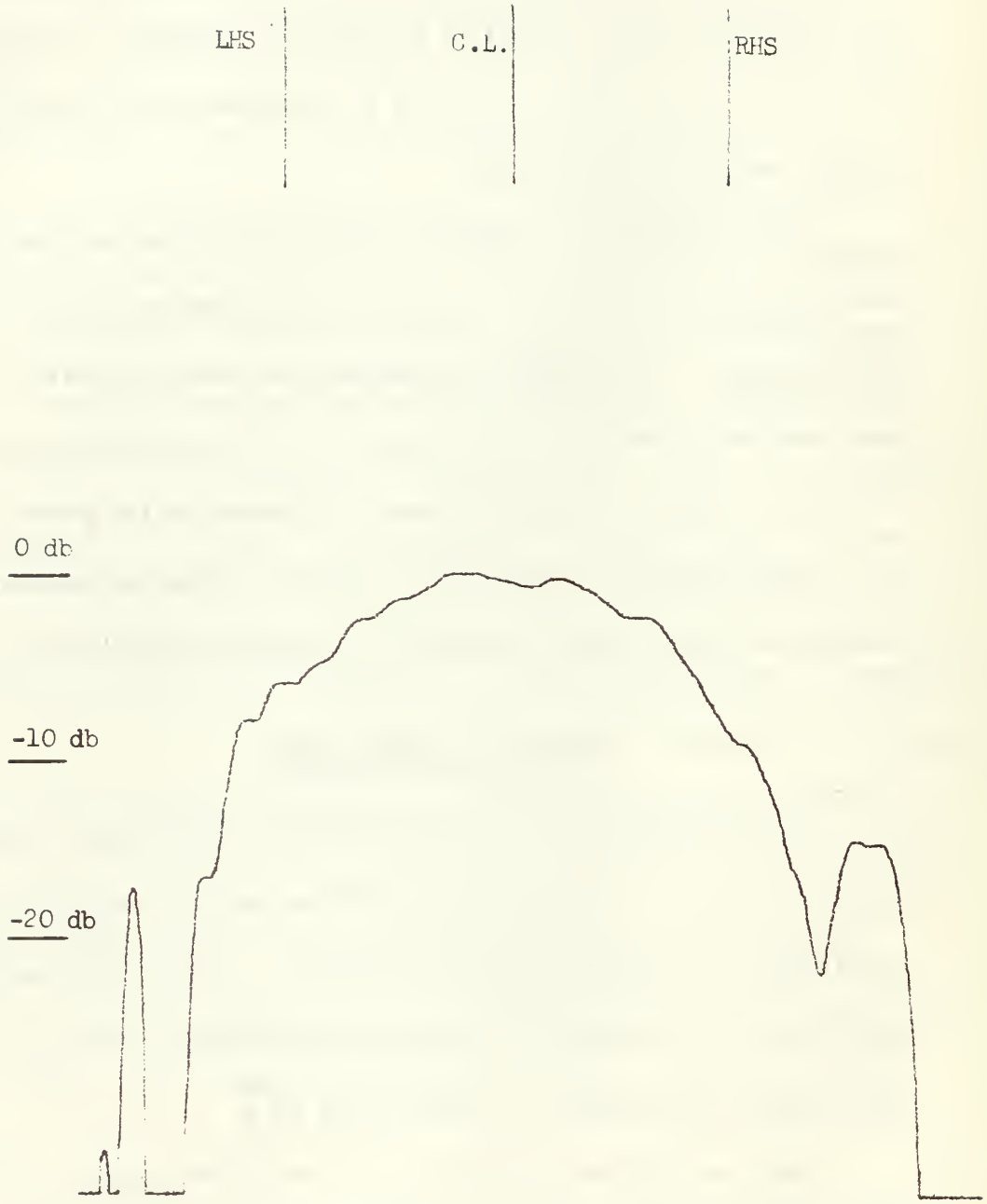

Far Field Pressure at Z = 51.0 cm for Barium Titanate Piston.

Figure 4.1

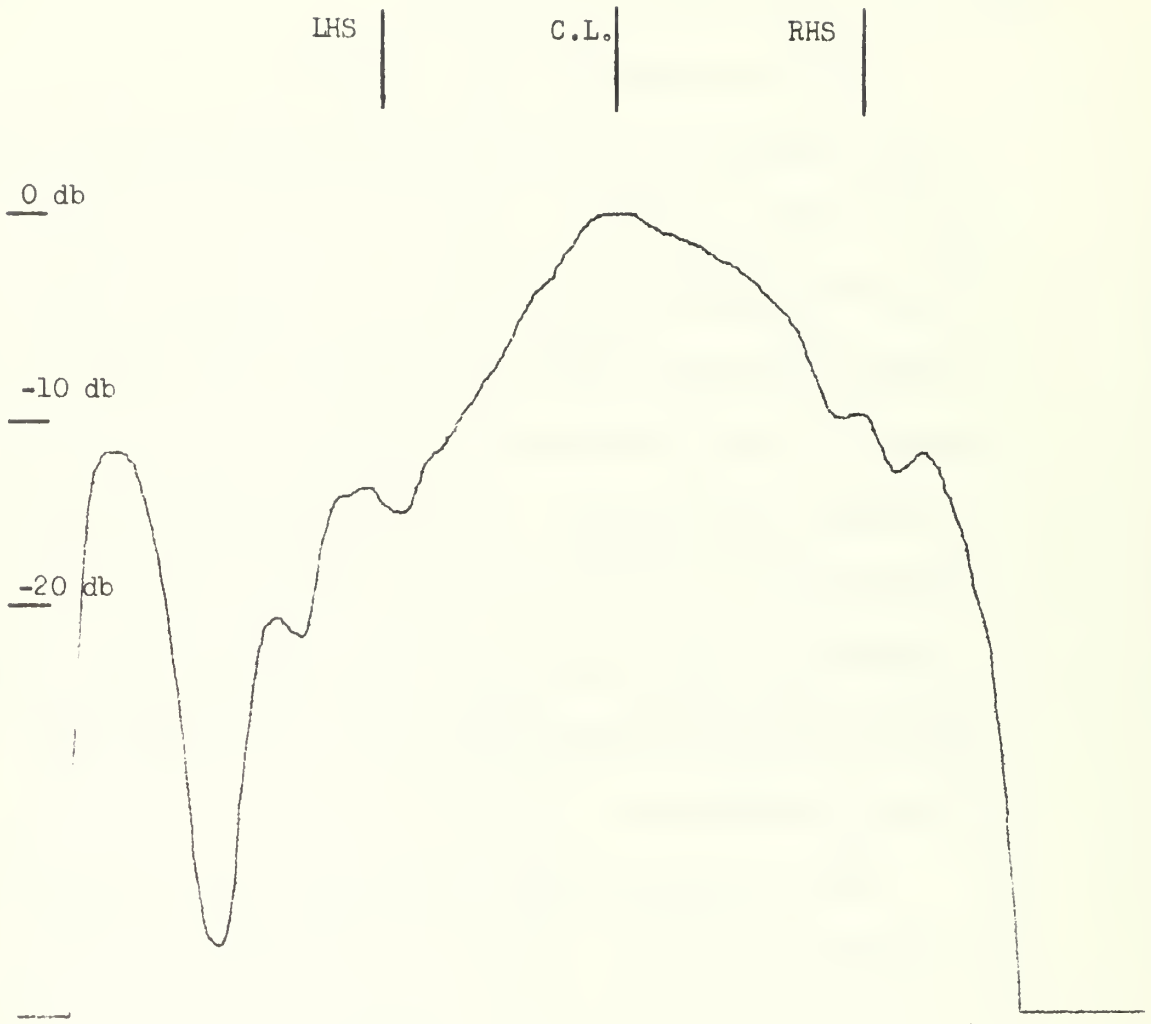

Far Field Pressure at Z = 51.0 cm for Mylar Piston.

Figure 4.2

behavior of the MYLAR transducer was attributed to fabrication faults in the construction of the transducer. It was noted, however, that the beam widths of the major lobes produced by the two transducers were approximately equal.

The two pressure level plots taken 7.0 cm from the face of source dramatically illustrated the near field differences between the two types of sources. The pressure level variations across the face of the Barium Titanate source are in excess of 50 db. Even though asymmetric, the pressure pattern of the ceramic source, Fig. 4.3, clearly illustrated the diffraction pattern associated with a constant velocity source. The pressure pattern produced by the MYLAR source, Fig. 4.4, did not exhibit variations anywhere comparable to those produced by the ceramic source. The maximum pressure level variations across the face of the MYLAR transducer at this distance were on the order of $\pm$ 5 db.

The near field pressure plots taken at 2.5 cm (Figs. 4.5 and 4.6) show the pressure variation for the Barium Titanate source to be on the order of 50 db while the pressure variations for the MYLAR sources are once again on the order of $\pm$ 5 db. Plots taken at 1.0 cm (Figs. 4.7 and 4.8) show the ceramic source pressure variations to be greater than 40 db while the pressure variations for the MYLAR source are $\pm$ 3 db. This sequence of pressure plots taken at 1.0, 2.5 and 7.0 cm from the face of the source indicated that the large differences between the near field pressure patterns produced by

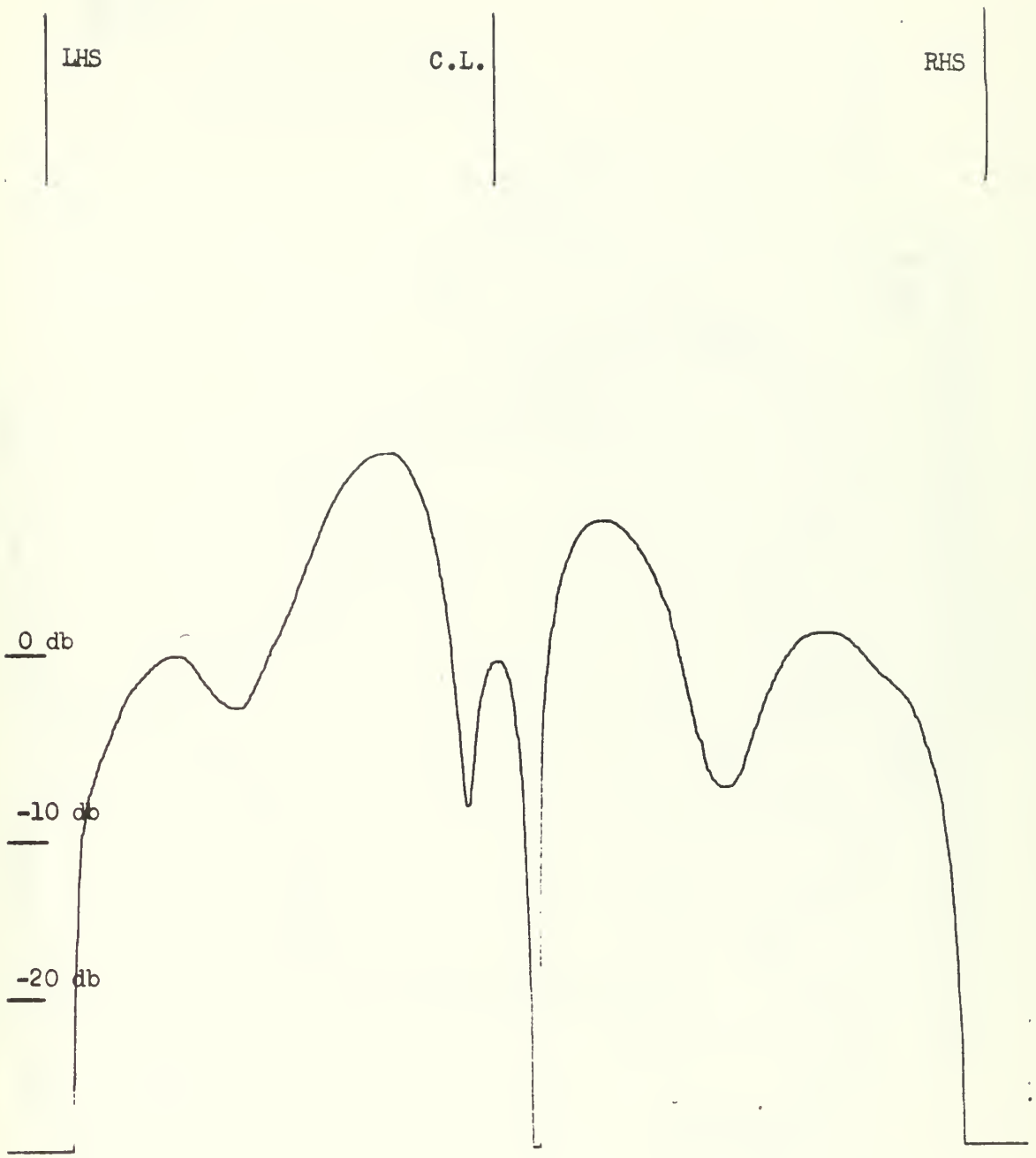

Near Field Pressure at Z = 7.0 cm for Barium Titanate Piston

Figure 4.3

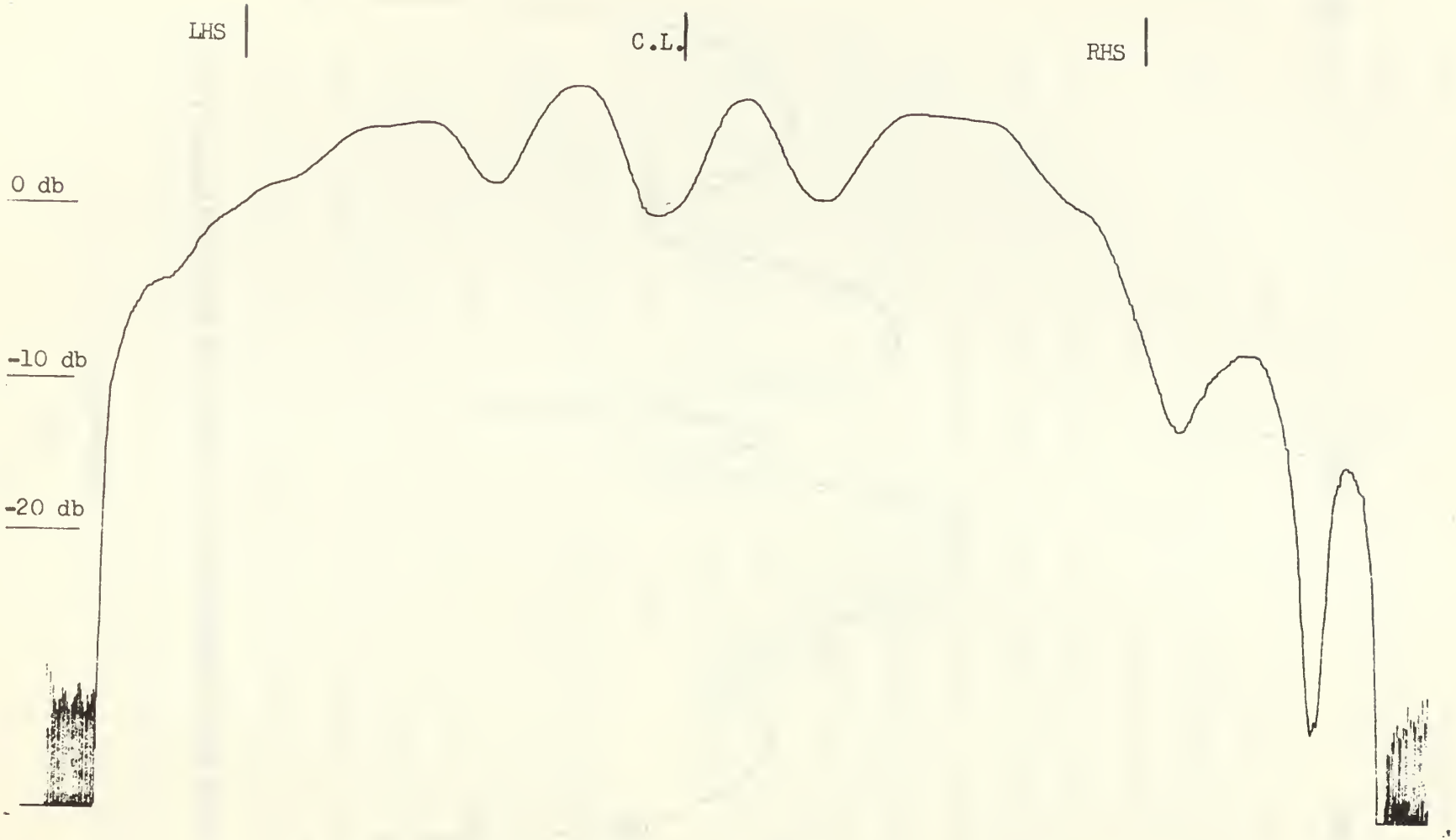

Near Field Pressure at Z = 7.0 cm for Mylar Piston

Figure 4.4

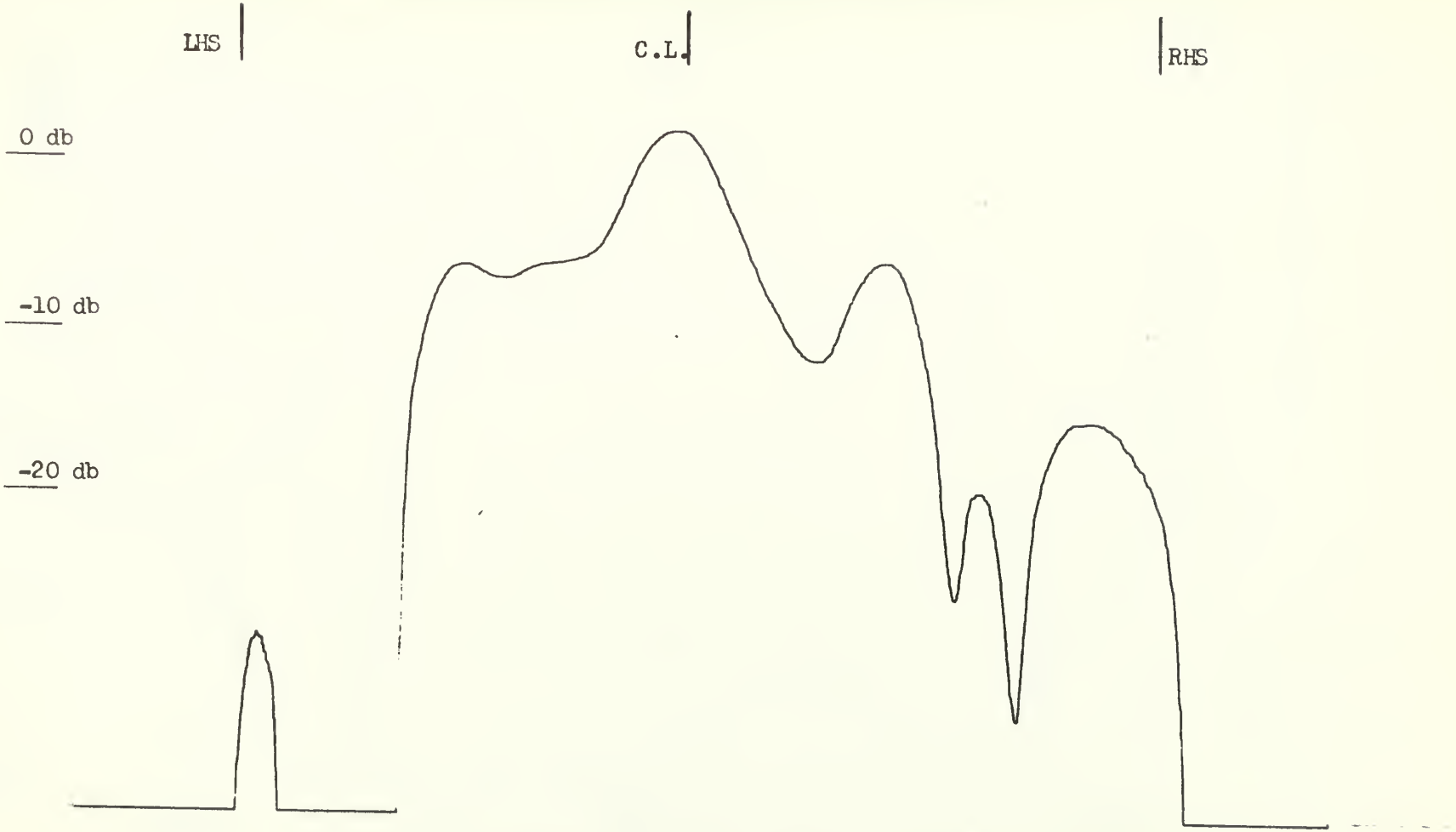

Near Field Pressure at Z = 2.5 cm for Barium Titanate Piston

Figure 4.5

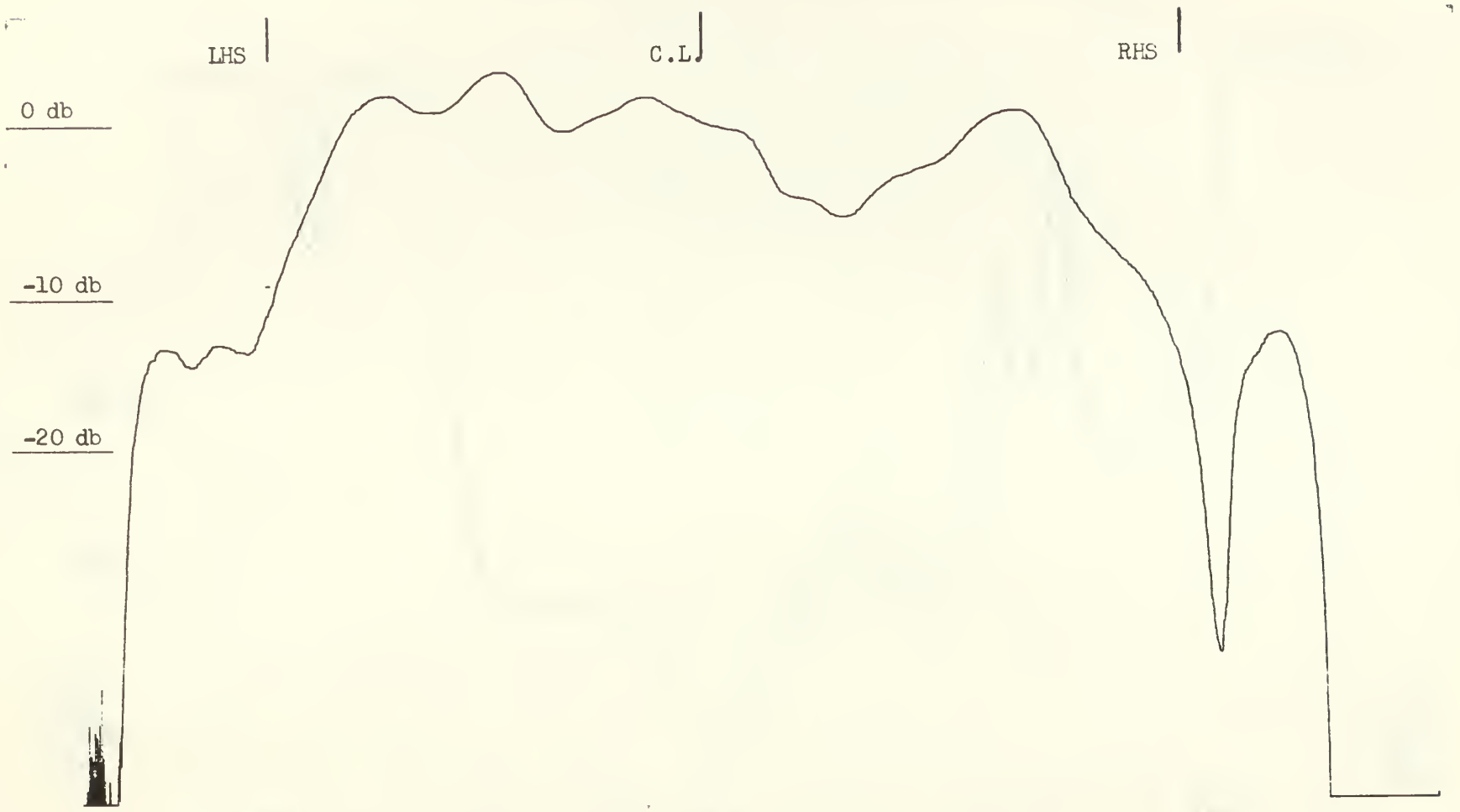

Near Field Pressure at Z = 2.5 cm for Mylar Piston

Figure 4.6

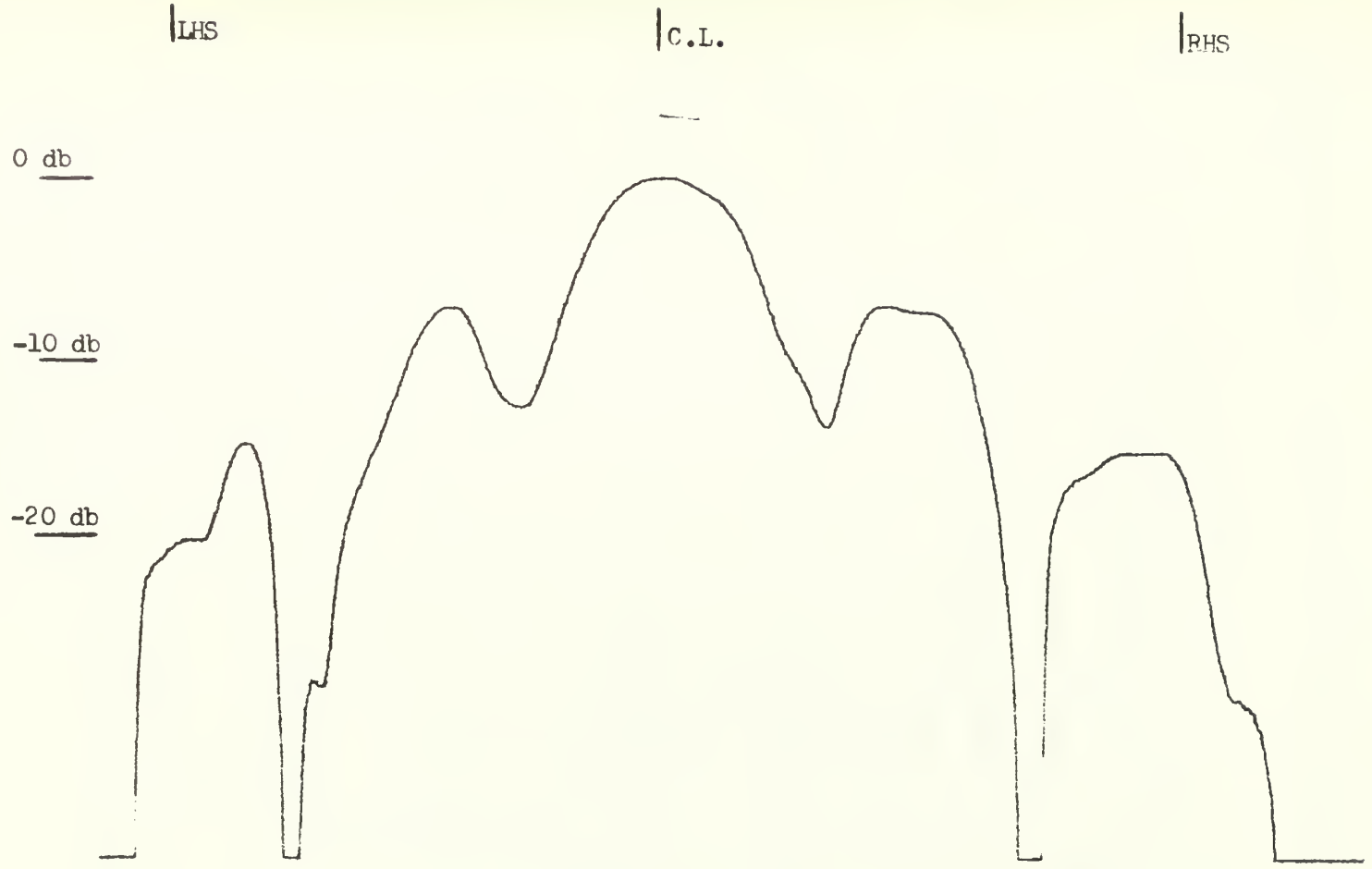

Near Field Pressure at Z = 1.0 cm for Barium Titanate Piston

Figure 4.7

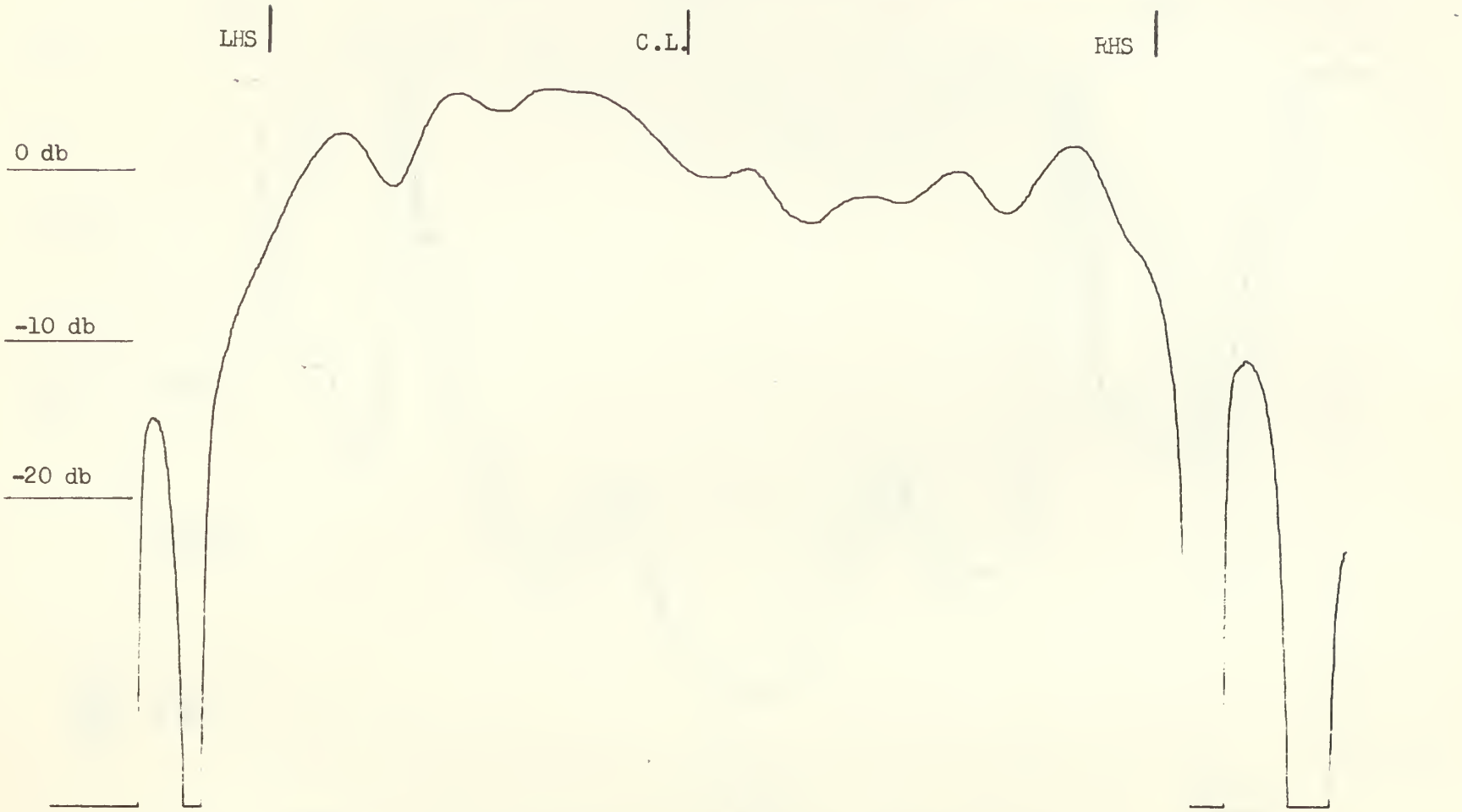

Near Field Pressure at Z = 1.0 cm for Mylar Piston

Figure 4.8

the two types of sources were observed for various distances from the sources. The relative smoothness of the pressure pattern produced by the MYLAR source suggested that this source behaved more like a constant pressure source than a constant velocity source.

In order to provide assurance that the asymmetries observed in the pressure patterns of the Barium Titanate source were not a function of the range variation encountered due to motion of the receiver, further plots were made. Initially, the receiver was placed 6.1 cm from the source and the tracks were aligned parallel to the face of the source. A plot of the pressure pattern was then made, Fig. 4.9. The source was then turned through an angle of approximately 5^{o} so that the receiver path clearly was not parallel to the transducer face. A plot of the pressure pattern was again made, Fig. 4.10. Figures 4.9 and 4.10 were compared and found to be essentially the same. The source was then restored to its original alignment, and the tracks were moved so that the path of the receiver was 5.9 cm away from the face of the transducer. A plot of the pressure pattern was once again made, Fig. 4.11. Comparison of Fig. 4.11 with 4.9 showed that the two plots are essentially the same. By virtue of the above process, it was reasoned that the plots taken were not essentially affected by the small variations in distance, $\pm$ 0.1 cm, encountered.

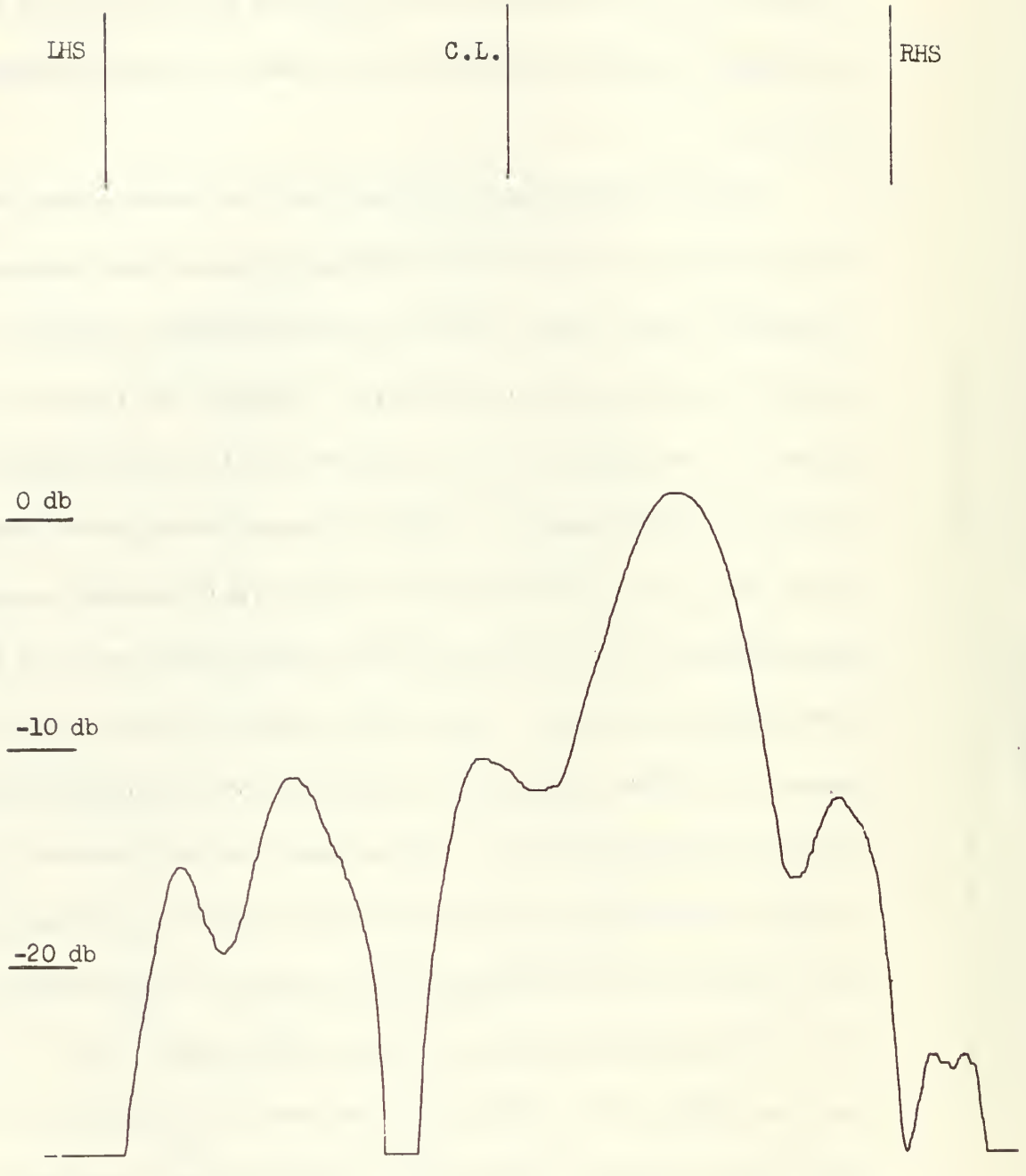

Near Field Pressure at Z = 6.1 cm for Barium Titanate Piston

Figure 4.9

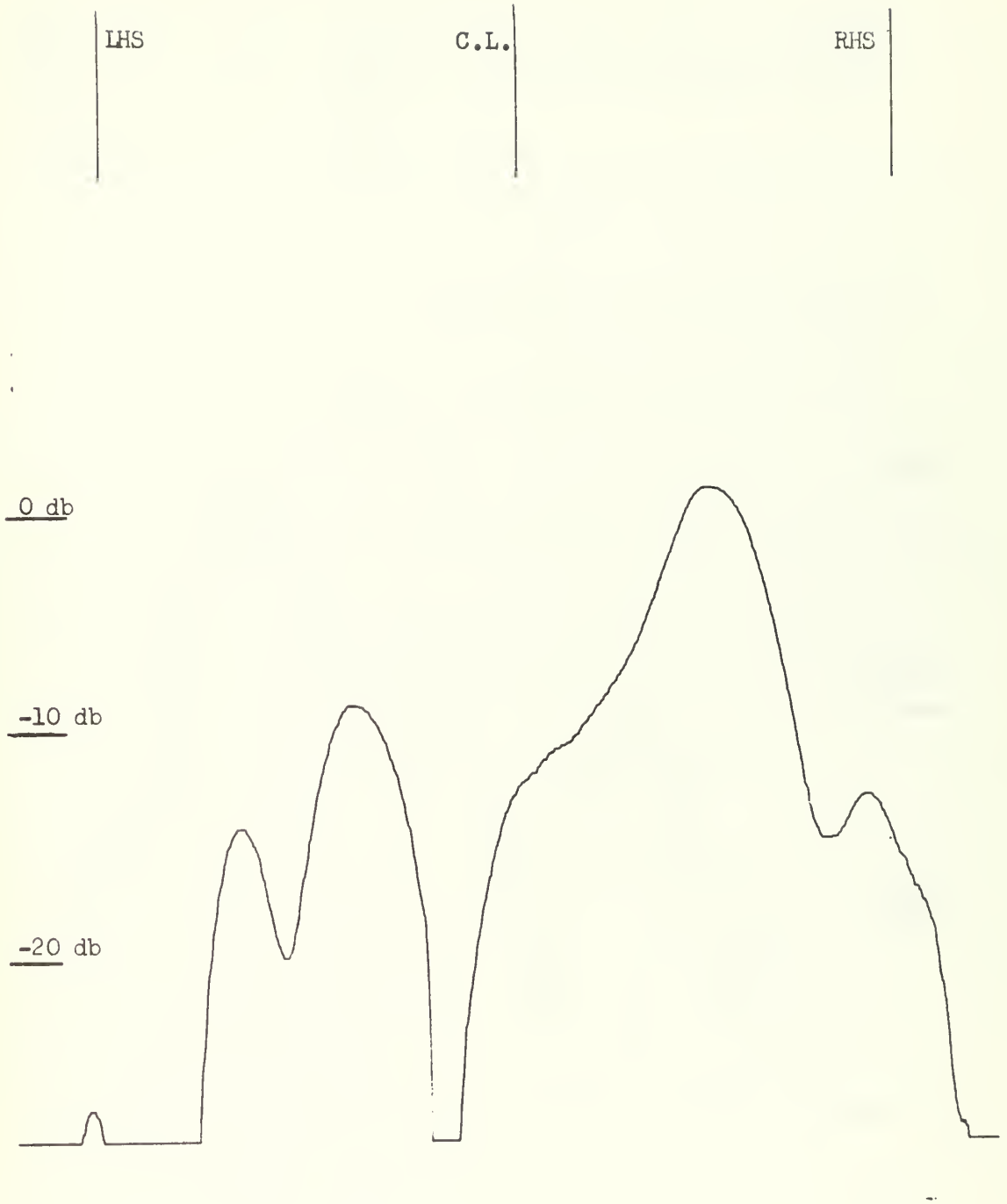

Near Field Pressure for Barium Titanate Piston with Z varying Between 5.6 and 6.6 cm

Figure 4.10

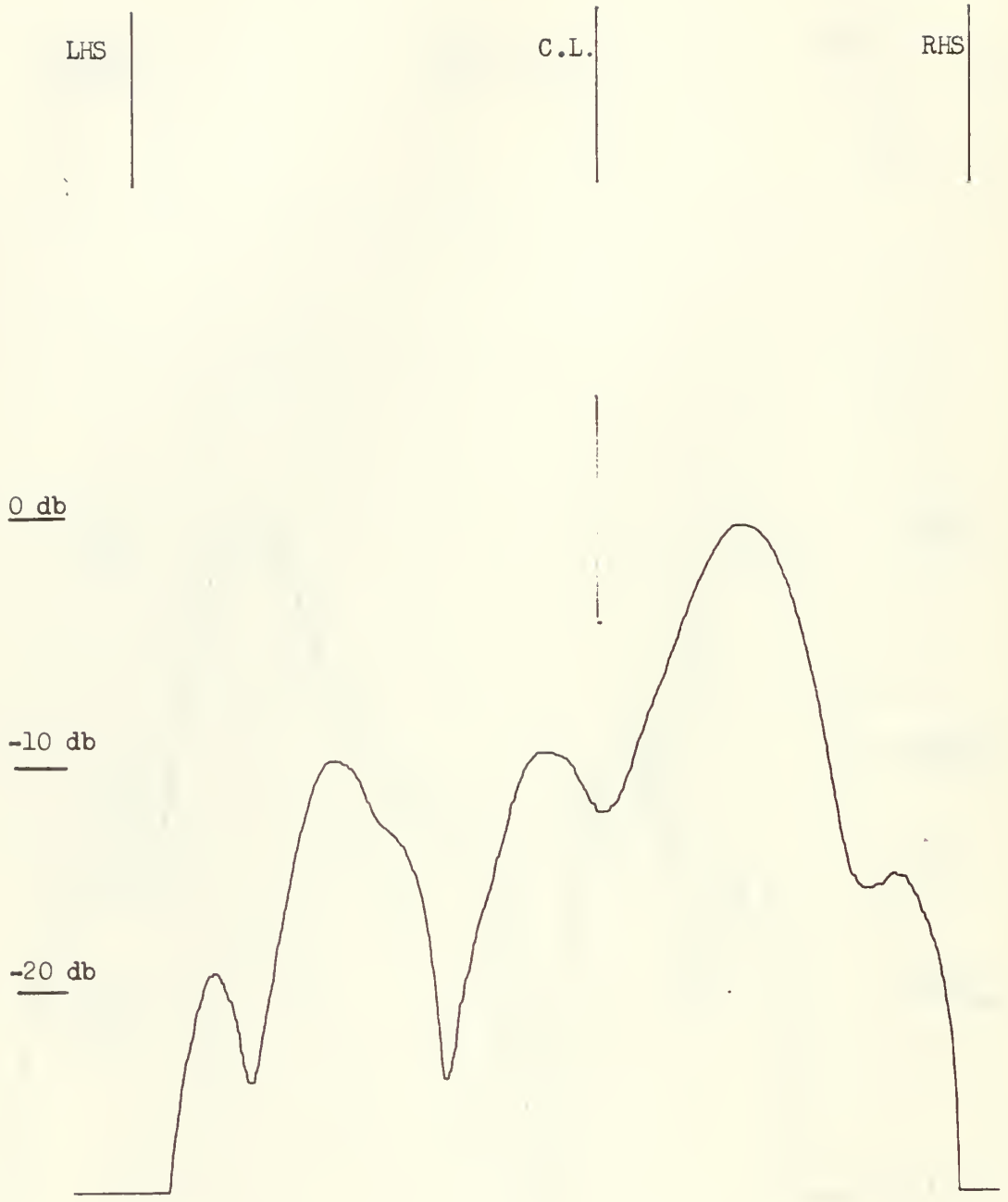

Near Field Pressure at Z = 5.9 cm for Barium Titanate Piston

Figure 4.11

Near field pressure plots were also made with the receiver positioned above and below the horizontal axis of the source. These plots, beyond verifying the intense asymmetries in the two units, did not provide any additional information and were therefore omitted from this research report.

5. CONCLUSIONS AND RECOMMENDATIONS

It is felt that in spite of the experimental difficulties encountered, it has been shown that the MYLAR transducers are definitely not constant velocity sources. Pressure level plots taken clearly suggest that the MYLAR transducer is very similar to a constant pressure source. Lack of developed theory and precise experimental data preclude one saying conclusively that the MYLAR is indeed a constant pressure source.

For future research in this area it is recommended that an array of small piezoelectric sources be used as the experimental model of a constant velocity piston. It is also recommended that computer programs be developed to map the near field pressure levels of a constant velocity and constant pressure circular pistons.

BIBLIOGRAPHY

1. G. L. Palatini, "Electroacoustic Properties of MYLAR Dielectric Underwater Sound Transducers", Thesis, Naval Postgraduate School, Monterey, Calif. (1966).

2. J.W.S. Rayleigh, The Theory of Sound, Volume II (Dover Publications, (1945).

3. L. V. King, "On the Acoustic Radiation Field of the Piezo-Electric Oscillator and the Effect of Viscosity on Transmission", Can. J. of Res. 135-155 (1934).

4. C.J. Bouwkamp, "A Contribution to the Theory of Acoustic Radiation", Philips Research Reports, 251-277 (1946).

5. M. Greenspan, "Baffled Piston Radiator: Expansion of Potential in Far, Paraxial Field", J. Acoust. Soc. Am., 40, 251-252 (1966).

6. H. Stenzel, "Ueber die Berechnaug der Schallfelder unmittelbar von einer kreisformigen Kolbenmembran", Ann. d. Phys. 41, 245-260 (1942).

7. H. Stenzel, Leitfaden zur Berechnung von Schallvorgangen (Springer - Verlag, Berlin, 1958).

8. A. Schoch, "Betrachtungen ueber das Schallfeld einer Kolbenmembran", Akust. Z. 6, 318-326 (1941).

9. A. O. Williams, Jr., and L.W. Labaw, "Acoustic Intensity Distributions from a 'Piston' Source", J. Acoust. Soc. Am., 16, 231-236 (1945).

10. A. O. Williams, Jr., "The Piston Source at High Frequencies", J. Acoust. Soc. Am., 23, 1-6 (1951).

11. A. H. Carter and A.O. Williams, Jr., "A New Expansion for the Velocity Potential of a Piston Source", J. Acoust. Soc. Am., 23, 179-184 (1951).

12. A.O. Williams, Jr., "Acoustic Field of a Circular Plane Piston", J. Acoust. Soc. Am., 36, 2408-2410 (1964).

13. A.O. Williams, Jr., "Medium and Far Field Expressions for Velocity Potential of Circular Plane Piston", J. Acoust. Soc. Am., 39, 1142-1144 (1966).

14. A. O. Williams, Jr., "Correction: Medium and Far-Field Expressions for Velocity Potential of Circula r Plane Piston", J. Acoust. Soc. Am., 41, 1549-1550 (1967).

15. H. Seki, A. Granato, and R. Truell, "Diffraction Effects in the Ultrasonic Field of a Piston Source and Their Importance in the Accurate Measurement of Attenuation", J. Acoust. Soc. Am., 28, 230-238 (1956).

16. G.N. Watson, A Treatise on the Theory of Bessel Functions (Cambridge University Press, Cambridge, 1945) 2nd Ed.

17. R.H. Quint, "Acoustic Field of a Circular Piston in the Near Zone", J. Acoust. Soc. Am., 31, 190-191 (1959).

18. A. B. Coppens, Private Communication (1968).

19. L. E. Kinsler and A. R. Frey, Fundamentals of Acoustics (John Wiley & Sons, Inc., New York, 1962) 2nd Ed.

20. Gulton Industries Inc., Glennite Piezoceramics, Bulletin H-500 (Metuchen, New Jersey).

21. W. C. Moyer, Private Communication (1968).

INITIAL DISTRIBUTION LIST

		No. Copies
1.	Defense Documentation Center Cameron Station Alexandria, Virginia 22314	20
2.	Library Naval Postgraduate School Monterey, California 93940	2
3.	Commander Naval Ships Systems Command Headquarters Washington, D. C. 20360	1
4.	Professor Alan B. Coppens Department of Physics Naval Postgraduate School Monterey, California 93940	1
5.	Professor Herman Medwin Department of Physics Naval Postgraduate School Monterey, California 93940	1
6.	Lieutenant Commander Toby G. Warson, USN USS QUEENFISH (SSN-651) FPO San Francisco, California 96601	1

DOCUMENT CONTROL DATA - R & D

Security classification of title, body of abstract and indexing annotation must be entered when the overall report is classified)

1. ORIGINATING ACTIVITY (*Corporate author*)

Naval Postgraduate School
Monterey, California 93940

2a. REPORT SECURITY CLASSIFICATION

Unclassified

2b. GROUP

3. REPORT TITLE

Investigation of the Boundary Conditions Applicable to Underwater, Air-Backed, Flexible-Diaphragm Transducers

4. DESCRIPTIVE NOTES (*Type of report and inclusive dates*)

Thesis - June 1968

5. AUTHOR(S) (*First name, middle initial, last name*)

Toby Gene WARSON

6. REPORT DATE	7a. TOTAL NO. OF PAGES	7b. NO. OF REFS
June 1968	66	21

8a. CONTRACT OR GRANT NO	9a. ORIGINATOR'S REPORT NUMBER(S)
b. PROJECT NO.	
c.	9b. OTHER REPORT NO(S) (*Any other numbers that may be assigned this report*)
d.	

10. DISTRIBUTION STATEMENT This document is subject to special export controls and each transmittal to foreign government or foreign nationals may be made only with prior approval of the Naval Postgraduate School.

11. SUPPLEMENTARY NOTES	12. SPONSORING MILITARY ACTIVITY
	Naval Postgraduate School Monterey, California 93940

13. ABSTRACT

The operation of the MYLAR electrostatic transducer used as a transmitter is studied theoretically and experimentally. A development is made of the mathematical solutions necessary to map the near field patterns generated by a constant velocity circular piston set on an infinite baffle and also a constant pressure piston in the same circumstances.

Boundary conditions applicable to the MYLAR piston are postulated based on equivalent circuits which allow investigation of the theoretical behaviors of the transducer. The postulated boundary conditions are then experimentally investigated. It is shown that an underwater, air-backed, flexible diaphragm transducer very closely approximates a "constant pressure" source.

14 KEY WORDS	LINK A		LINK B		LINK C	
	ROLE	WT	ROLE	WT	ROLE	WT
Underwater Transducers						
MYLAR Transducers						
Electrostatic Transducers						
Acoustic Sources						
Constant Velocity Source						
Constant Pressure Source						
Flexible Diaphragm Transducer						